PHYSICAL REVIEW B **85**, 125304 (2012)

Coherent spin dynamics of electrons and holes in semiconductor quantum wells and quantum dots under periodical optical excitation: Resonant spin amplification versus spin mode locking

I. A. Yugova,[1,2] M. M. Glazov,[3] D. R. Yakovlev,[1,3] A. A. Sokolova,[2] and M. Bayer[1]
[1]*Experimentelle Physik 2, Technische Universität Dortmund, 44221 Dortmund, Germany*
[2]*Physical Faculty of St.Petersburg State University, 198504 St. Petersburg, Russia*
[3]*Ioffe Physical-Technical Institute, Russian Academy of Sciences, 194021 St. Petersburg, Russia*
(Received 29 December 2011; published 12 March 2012)

The coherent spin dynamics of resident carriers, electrons, and holes in semiconductor nanostructures is studied theoretically under the conditions of periodical optical excitation using short laser pulses and in an external magnetic field. The generation and dephasing of spin polarization in an ensemble of carrier spins, for which the relaxation time of individual spins exceeds the repetition period of the laser pulses, are analyzed. Accumulation of the spin polarization is manifested either as resonant spin amplification or as mode locking of carrier spin coherences. It is shown that both regimes have the same origin, while their appearance is determined by the optical pump power and the spread of spin precession frequencies in the ensemble.

DOI: 10.1103/PhysRevB.85.125304 PACS number(s): 78.67.−n, 78.47.−p, 71.35.−y

I. INTRODUCTION

The coherent spin dynamics of carriers in semiconductor nanostructures attract considerable attention nowadays due to future quantum information technologies based on spintronics applications.[1–3] With respect to fundamental studies, this research field delivers exciting and unexpected results on the properties of spin systems and the possibility to control them by external fields or by structural parameters.

Optical pump-probe technique for time-resolved Faraday and Kerr rotation is based on generation of spin polarization by trains of laser pulses, where the pulse durations range from hundreds of femtoseconds to a few picoseconds. It has been proven to be among the most reliable tools for investigating coherent spin dynamics in semiconductor nanostructures.[1,4–16] The principle of this magneto-optical technique is the following: an intense laser pulse of circularly polarized light (the pump) is used to orient spins and, therefore, to create a macroscopic spin polarization.[17] This polarization is probed by the linearly polarized probe pulses, which rotate their polarization plane after propagation through the spin-polarized medium (Faraday rotation effect) or reflection at this medium (Kerr rotation effect). The probe pulse is time delayed relative to the pump pulse, and by tuning this delay, one can measure the spin polarization dynamics. To study the coherent spin dynamics, the sample is exposed to an external magnetic field, typically oriented perpendicular to the light wave vector (Voigt geometry), which allows one to detect the precession of the optically induced spin polarization and monitor its decay. Application of the pump-probe technique to single spins, which is potentially possible,[18,19] is demanding. Studying spin ensembles that contain millions of carrier spins is much more convenient.[14,15,20]

In pump-probe experiments, the spin dynamics evolution is typically measured over times shorter than the repetition period of the pump pulses, which is about 13 ns for commonly used mode-locked Ti:sapphire lasers emitting pulses at a repetition rate of 75–80 MHz. It has been shown experimentally that in bulk semiconductors, quantum wells (QWs), and quantum dots (QDs), the carrier spin relaxation time can substantially exceed the repetition period.[20,21] In this case, the spin polarization induced by subsequent pump pulses can accumulate if a phase-synchronization condition is fulfilled for the precessing carrier spins. It results in two effects: resonant spin amplification (RSA), observed in bulk and QW spin systems with a relatively small dispersion of precession frequencies, and spin mode locking (SML) found for an ensemble of singly charged QDs with a large dispersion of Larmor frequencies (see, e.g., Refs. 20 and 21 and references therein).

For studying the RSA regime experimentally, scanning the magnetic field has been suggested instead of the commonly used scan of the pump-probe time delay.[5] The probe pulse arrival time in this case is fixed at a small negative delay prior to the pump pulse arrival. The resulting RSA spectrum is a periodic function of magnetic field from which information on carrier g factor and dephasing time of the spin ensemble can be obtained.

In this paper, we show that the RSA and SML are two different manifestations of the same phenomenon: spin accumulation caused by the periodic excitation with pump pulse trains. We elaborate the fundamental differences in conditions for appearance of these two regimes. The most important parameters in this regard are the pump power and the spin precession frequency spread causing spin dephasing. Differences of the two parameters, in turn, lead to different phenomenologies in experiment, providing significantly different capabilities for analyzing spin systems quantitatively.

The paper is organized as follows. In Sec. II, we recall the basic concepts and equations for describing spin coherence generation. We discuss the difference between the classical and quantum mechanical approaches to describing carrier spin coherence generation for resonant trion excitation. Then, we consider generation of long-lived spin coherence during the trion lifetime. We describe the spin dynamics of charged carriers and trions in magnetic field and discuss the effects of spin relaxation and spin precession of the trion spin on the long-lived spin coherence of resident carriers. We also consider here the long-lived spin dynamics after generation and the spin accumulation caused by the train of pump pulses. Section III is devoted to the RSA regime, for which we consider different effects: trion spin relaxation, nuclear field fluctuations, and spin relaxation anisotropy. The conditions, which are

important for observing RSA, and the characteristics, which one can extract from the analysis of RSA signals, are collected at the end of Sec. III. Section IV describes the main features of the mode locking of electron spin coherences. Then, in Sec. V we compare the spin dynamics in the RSA and SML regimes, obtain conditions for the SML regime, and discuss the transition to the RSA regime. In the Conclusions, we give a comparative description of the RSA and SML regimes and their applicability to investigations of long-lived spin dynamics in low-dimensional systems.

II. GENERATION OF SPIN COHERENCE

In the following, we analyze the long-lived spin coherence of resident carriers (electrons and holes) generated by periodic light excitation in semiconductor quantum wells and quantum dots. We consider a situation with a low concentration of resident carriers when the probability to have two charge carriers with significantly overlapping wave functions is negligible. In this case, mainly few-particle complexes, excitons (electron-hole pairs), and trions (three-particle complexes) can be optically excited, while other many-body correlations are negligible. For quantum wells, this corresponds to typical carrier densities smaller than 10^{10} cm^{-2} for which, at liquid-helium temperatures, carriers are localized on QW width fluctuations with respect to their in-plane motion. Only one carrier per localized site is typical for such concentrations, and the distance between the localized carriers exceeds the extensions of neutral and charged exciton wave functions. For quantum dots, the low-concentration regime corresponds to occupation of a dot with only one resident carrier, i.e., to a regime of singly charged QDs.

Here, we consider the theoretical aspects of the problem. We do not discuss the experimental aspects of the observations (measurements) of long-lived spin coherences and features of ellipticity and Faraday rotation signals. We limit ourselves to the degenerate pump-probe regime, when the probe laser has the same photon energy as the pump one, and to resonant excitation of the trion states. We assume that the pulse duration is significantly shorter than all characteristic relaxation times of the considered spin system. These conditions are typical for experiments with semiconductor nanostructures.[1,4] Other regimes are studied in detail elsewhere.[22–25]

For low concentrations of resident carriers, charged excitons (trions) play an important role in the generation process of carrier spin coherence.[9,15] A negatively charged exciton (T^- trion) is a bound state of two electrons and one hole, while a positively charged exciton (T^+ trion) is a bound state of two holes and one electron. The trion ground state at zero magnetic field has a singlet spin configuration, such that the spins of the two identical carriers are aligned opposite to each other and the trion Zeeman splitting is controlled by the g factor of the unpaired carrier, e.g., the hole in T^-. Hereinafter, we assume that only heavy holes with angular momentum projections $\pm 3/2$ onto the growth axis are involved.

The theoretical analysis used in this paper can be equally applied to structures with resident electrons or resident holes. In order to do that, we introduce universal notations: the resident carrier spin $\boldsymbol{S}$, the trion spin $\boldsymbol{S}^T$, the Larmor frequency of the resident carrier $\omega = g\mu_B B/\hbar$, and the Larmor frequency of the trion $\Omega = g_T\mu_B B/\hbar$. Here, $\boldsymbol{B}$ is the external magnetic field, μ_B is the Bohr magneton, g and g_T are the g factors of the resident carrier and trion, respectively. Similarly, universal notations are also used in what follows to denote characteristic time scales.

In n-type doped structures with resident electrons, $\boldsymbol{S}$ is the electron spin, $\boldsymbol{S}^T$ is a (pseudo)spin of the T^- trion ($S^T = +1/2$ for $+3/2$ hole and $-1/2$ for $-3/2$ hole), ω is the electron Larmor frequency, and Ω is the T^- Larmor frequency determined by the hole g factor. Correspondingly, in p-type doped structures with resident holes, $\boldsymbol{S}$ is the heavy-hole pseudospin, $\boldsymbol{S}^T$ is the spin of the T^+ trion, which corresponds to the electron spin in this trion, ω is the heavy-hole Larmor frequency, and Ω is the T^+ Larmor frequency determined by the electron g factor.

Note that the quantities $\boldsymbol{S}$ and $\boldsymbol{S}^T$ can refer either to a single spin of resident electron (hole) and trion in, e.g., an individual quantum dot, or to the averaged values characterizing ensembles of identical dots. The latter means that all spins in such ensembles have the same g-factor value and, therefore, precess in magnetic field in phase with each other with the same Larmor frequency. In those cases, where ensemble inhomogeneity is important, we will specify explicitly how the averaging over the spin precession frequencies spread is done.

For the sake of simplicity, we consider in most parts of this paper n-type doped structures with resident electrons, as there are more experimental data available for these structures. Wherever we analyze p-type doped structures, this will be noted. Before we proceed to the analysis of spin precession in magnetic field and spin dephasing processes, let us inspect briefly the models of optical generation of spin coherence.

A. Resonant excitation of trion: Classical and quantum mechanical approaches to carrier spin coherence generation

The singlet trion state, being excited resonantly by the laser pulse, plays an important role in the spin coherence generation. The trion generation probability for resonant excitation depends on the light polarization and the spin orientation of the resident carrier. For instance, in n-type doped structures, a σ^+ polarized pump generates a hole with spin projection $+3/2$ onto the light propagation axis z and an electron with spin projection $-1/2$. Therefore, trion formation is possible only when the resident electron has spin projection $+1/2$. As a result, the circularly polarized pump pulse selects electrons with particular spin orientation from the ensemble of resident electrons to form trions. This, in turn, leads to spin polarization of the resident electrons.

There are two approaches for describing the spin coherence generation by circularly polarized light pulses.[25] The first one is essentially quantum mechanical: a singly charged QD or a QW with a localized resident electron is modeled as a two-level system.[8,15,23,26] The ground state corresponds to the resident electron, while the excited state is the singlet trion [see Fig. 1(a)].

The interaction of the two-level system with the resonant pump pulse depends on the pulse parameters (polarization, intensity, and pulse duration) and on the level occupations.

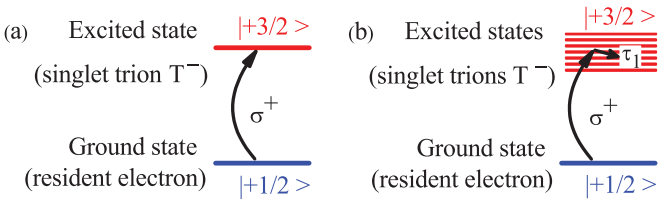

FIG. 1. (Color online) (a) Scheme of transitions for a strongly localized electron (e.g., in a singly charged quantum dot). The initial state for the optical transition is a resident electron and the final state is a singlet trion T^-. This scheme is consistent with the quantum mechanical approach. (b) Scheme of transitions for the case of weakly localized resident carriers (e.g., in a quantum well with a low-density electron gas); τ_1 denotes the scattering time between different trion states. This scheme is consistent with the classical approach.

The pump pulse action time τ_p is assumed to be the shortest of all time scales in the problem, namely, the trion dephasing and scattering times, the electron Larmor precession period, the trion radiative lifetime, the spin dephasing and decoherence times, etc. Under typical experimental conditions, the trion lifetime is much shorter than the pump pulse repetition period and, consequently, trion spin polarization is absent considerably before the next pump pulse, i.e., is not detectable at small negative time delays. It follows then that the resident carrier spin pseudovector $\boldsymbol{S} = (S_x, S_y, S_z)$ before the pump pulse $\boldsymbol{S}^b$ and after the pump pulse $\boldsymbol{S}^a$ are related to each other through[23]

$$S_z^a = \pm\frac{Q^2-1}{4} + \frac{Q^2+1}{2} S_z^b\,, \tag{1a}$$

$$S_x^a = Q\cos\Phi S_x^b \pm Q\sin\Phi S_y^b\,, \tag{1b}$$

$$S_y^a = Q\cos\Phi S_y^b \mp Q\sin\Phi S_x^b\,, \tag{1c}$$

where the top (bottom) sign + (−) corresponds to σ^+ (σ^-) polarized pump pulses in n-type structures and to σ^- (σ^+) pulses for p-type structures, respectively. Similar sign definition (top sign corresponds to σ^+ excitation of n-type structure) is used hereinafter in Eqs. (2), (3), and (4). The parameters $0 \leqslant |Q| \leqslant 1$ and $0 \leqslant \Phi < 2\pi$ characterize the pump pulse area and the spectral detuning of the pulse from the trion resonance. The explicit expressions for these quantities are given in Ref. 23. For the resonant pump pulse $\Phi = 0$ and $Q = \cos(\Theta/2)$, where Θ is the pump pulse area: $\Theta = \int 2|\langle d\rangle E(t)|dt/\hbar$. Here, $\langle d\rangle$ is the dipole transition matrix element and $E(t)$ is the smooth envelope of the electric field of the laser pulse. The z component of the trion spin pseudovector after, e.g., a σ^+ pump pulse in an n-type system or a σ^- pump pulse in a p-type system is given by[23]

$$S_z^{T,a} = S_z^b - S_z^a = \frac{1-Q^2}{4}\left(2S_z^b \pm 1\right). \tag{2}$$

Such an approach has been proven to be appropriate for the description of spin coherence generation in n-type singly charged QDs.[15] At low pump powers, where $\Theta \ll 1$, the additive contribution to the electron spin z component equals to

$$S_z^a - S_z^b = \mp\frac{\Theta^2}{16} \propto P, \tag{3}$$

where P is the pump pulse power. One of the main predictions of the considered quantum mechanical approach is that for high pump powers, the electron spin z component depends periodically on the pump area, i.e., shows Rabi oscillations inherent to a two-level system (see, e.g., Refs. 14, 15, and 27).

Another approach to describe spin coherence generation is based on the classical model, where the ensemble of electron spins is considered. Optical pulse leads to the trion formation, which involves participation of resident electrons with certain spin orientations. The initially unpolarized ensemble of the resident electrons becomes therefore spin polarized, at least at times shorter than the trion lifetime. Under certain conditions, which will be analyzed in detail below, e.g., efficient trion spin relaxation or fast Larmor precession of the resident electron spins, this induced spin polarization will present even after trion recombination.

For low pump powers, the total spin of resident electrons right after the pump pulse $S_z^{\rm tot}$ is proportional to the number of photogenerated trions and scales linearly with the pump pulse power.[9] In this limit, classical and quantum mechanical models agree with each other. For higher pump pulse powers in the classical model, the total electron spin saturates at the value

$$S_{z,\max}^{\rm tot} = \mp N/4, \tag{4}$$

where N is the total number of resident electrons in the system. The amount of trions formed for resonant excitation of the initially unpolarized electron ensemble can not exceed $N/2$ since only half of the resident electrons have suitable spin orientation to become excited to trion singlets. The other $N/2$ of the resident electrons, which are not captured to trions, have become fully polarized. In the classical model, Rabi oscillations inherent to two-level systems are absent.

The applicability of the classical model to the quantum-well structures is related to the weaker localization of electrons and trions on quantum-well imperfections. As a result, the generated trions can scatter to another localized state or to free trion states, as schematically illustrated in Fig. 1(b). The optical coherence of the trion with the pump is lost due to this scattering, while spin coherence is preserved. As a result, if the scattering time between different trion states τ_1 is considerably shorter than τ_p, the Rabi oscillations at high pump powers vanish[28] because the population of the excited state of the two-level system coupled to the optical pulse is small. At the same time, the spin polarization generated by the pump pulse can be substantial because spin does not relax during scattering. It corresponds to the experimental situation studied in Refs. 9 and 28.

It will be shown in Sec. III A that the quantum mechanical and classical approaches give the same results at low pump powers. Subsequently, we will use the quantum mechanical approach because it gives good descriptions for spin coherence generation for QDs in any excitation power regime and for QWs in the low power excitation regime.

B. Generation of long-lived spin coherence during the trion lifetime: Spin dynamics of charged carriers in magnetic field

1. Spin dynamics of resident carrier and trion

Right after the excitation pulse, the coupled dynamics of resident carrier spin $\boldsymbol{S}$ and trion spin $\boldsymbol{S}^T = (S_x^T, S_y^T, S_z^T)$ can be described by the following system of equations[9,15,23,26]:

$$\frac{d\boldsymbol{S}^T}{dt} = \frac{\mu_B}{\hbar}[g_T \boldsymbol{B} \times \boldsymbol{S}^T] - \frac{\boldsymbol{S}^T}{\tau_s^T} - \frac{\boldsymbol{S}^T}{\tau_r}, \tag{5a}$$

$$\frac{d\boldsymbol{S}}{dt} = \frac{\mu_B}{\hbar}[g\boldsymbol{B} \times \boldsymbol{S}] - \frac{\boldsymbol{S}}{\tau_s} + \frac{S_z^T \boldsymbol{e}_z}{\tau_r}. \tag{5b}$$

Here, $\boldsymbol{e}_z$ is the unit vector along the z axis. The magnetic field $\boldsymbol{B}$ is assumed to be parallel to the x axis. τ_s^T is the trion spin relaxation time, τ_s is the phenomenological spin relaxation time of the resident carrier,[29] and τ_r is the trion radiative lifetime. It is worth to mention that the carrier returning after the trion recombination is polarized either parallel or antiparallel to the z axis due to the optical selection rules [see the last term $\propto S_z^T \boldsymbol{e}_z$ in Eq. (5b)]. Note, that Eqs. (5) are equally applicable to the single quantum dot or to the ensemble of identical quantum dots.

It follows from Eqs. (5) that the carrier spin projection onto the magnetic field S_x is conserved. Introducing the trion spin lifetime $\tau_T = \tau_s^T \tau_r/(\tau_s^T + \tau_r)$, we arrive at the following expression for the transverse carrier spin component $S_+ = S_z + \mathrm{i}S_y$ (Ref. 15):

$$S_+(t) = S_+^a e^{-\mathrm{i}\omega t - t/\tau_s} + S_z^{T,a}[-\xi e^{-\mathrm{i}\omega t - t/\tau_s} + e^{-t/\tau_T}(\xi \cos \Omega t + \chi \sin \Omega t)]. \tag{6}$$

Here, the subscript a denotes the spin components at time $t = 0$ when the pump pulse is finished, e.g., $S_+^a = S_z^a + \mathrm{i}S_y^a$:

$$\xi = \xi_1 + \mathrm{i}\xi_2 = \frac{\mathrm{i}\omega/\gamma - 1}{\gamma\tau_r[(1 - \mathrm{i}\omega/\gamma)^2 + (\Omega/\gamma)^2]}, \tag{7}$$

$$\chi = \chi_1 + \mathrm{i}\chi_2 = \frac{\Omega/\gamma}{\gamma\tau_r[(1 - \mathrm{i}\omega/\gamma)^2 + (\Omega/\gamma)^2]}, \tag{8}$$

and $\gamma = \tau_T^{-1} - \tau_s^{-1} > 0$.

In order to have a closed equation system (5), we have to relate the carrier and trion spins at $t = 0$. This can be done through Eqs. (1) and (2). After a single pump pulse ($\boldsymbol{S}^b = 0$), one has

$$S_z^{T,a} = -S_z^a.$$

The first term in the right-hand side of Eq. (6) describes the carrier spin precession. The term proportional to $S_z^{T,a} e^{-\mathrm{i}\omega t}$ describes the spin polarization of the carrier returning after trion recombination. In the following, we consider the relation of these two contributions as a function of spin system parameters and external conditions.

2. Effect of trion spin relaxation on spin coherence of resident carrier

In the absence of an external magnetic field, the efficiency of resident carrier spin coherence generation is solely determined by the trion spin relaxation.[8,9,30] This becomes clear from Eq. (6), which for $B = 0$ reduces to

$$S_z(t) = S_z^a e^{-t/\tau_s} + S_z^{T,a}\xi(-e^{-t/\tau_s} + e^{-t/\tau_T}). \tag{9}$$

It follows from Eq. (7) that $\xi = -(\tau_r\gamma)^{-1} \approx -(1 + \tau_r/\tau_s^T)^{-1}$, provided that the carrier spin relaxation time exceeds by far both trion recombination time and trion spin lifetime. These conditions are readily fulfilled in experiment. Hence, the long-lived carrier spin coherence is given by

$$S_z(t) = (S_z^a - S_z^{T,a}\xi)e^{-t/\tau_s}, \quad t \gg \tau_T. \tag{10}$$

If spin relaxation in the trion is suppressed, i.e., $\tau_s^T \gg \tau_r$, then $\xi \to -1$. Therefore, since for a single pump pulse $S_z^{T,a} = -S_z^a$, the contribution of the carrier left behind the trion recombination compensates exactly the induced spin polarization of the resident carriers. As a result, no long-lived spin coherence for resident carriers is generated. In general, when the resident carrier has been polarized before pump pulse arrival, this carrier polarization will not be affected by the pump pulse and conserved after trion recombination. To conclude, trion spin relaxation is required to give rise to a nonzero long-lived spin coherence of the resident carriers in absence of a magnetic field.

3. Spin precession of resident carrier

Here, we dwell on the Larmor precession of the resident carriers, i.e., those which do not participate in trion formation. Spin precession of these carriers results in an imbalance of the spins of resident electrons and those returned from the trions after their recombination. Hence, the long-lived spin coherence can be excited even in the absence of trion spin relaxation. Provided that the trion spin does not precess,[31] $\Omega = 0$, the long-lived carrier spin coherence is given by[9]

$$S_z(t) = \mathrm{sign}\left(S_z^a\right)\left|S_z^a - S_z^{T,a}\xi\right|e^{-t/\tau_s}\cos(\omega t - \varphi), \quad t \gg \tau_T \tag{11}$$

where φ is the initial phase, which can be related to the parameter ξ (see Ref. 9 for details). Note that in Ref. 9 the phase is shifted by $\pi/2$ with respect to our definition in Eq. (11). The amplitude of the long-lived spin coherence $\mathcal{A}_s$ after a single pump pulse can be recast as

$$\mathcal{A}_s = \left|S_z^a - S_z^{T,a}\xi\right| = \left|S_z^a(1 + \xi)\right| \approx \left|S_z^a\right|\frac{|\omega\tau_r|}{\sqrt{1 + (\omega\tau_r)^2}}, \tag{12}$$

wherethe latter approximate equality is valid for a long trion spin relaxation time fulfilling the relation $\tau_s^T \gg \tau_r$. According to Eq. (12), the long-lived spin amplitude first increases with an increase of the magnetic field $\propto \omega\tau_r$ and then saturates in strong fields.

The general case of arbitrary $\omega\tau_r$ and τ_r/τ_s^T is illustrated in Fig. 2. Figure 2(a) demonstrates the dependence of the long-lived spin coherence amplitude $\mathcal{A}_s$ on magnetic field (expressed as ω/γ) for different values of the ratio τ_r/τ_s^T. Depending on the parameter τ_r/τ_s^T, the change of amplitude $\mathcal{A}_s$ as function of magnetic field (through $\omega \sim B$) occurs for different field values since γ itself is determined by τ_r and τ_s^T.

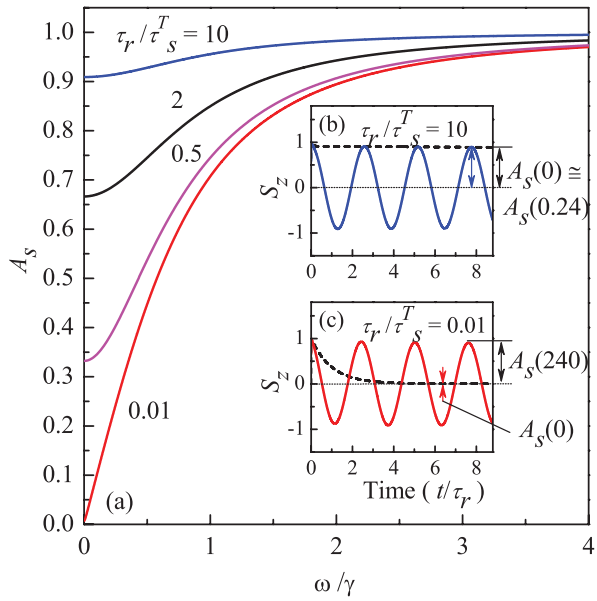

FIG. 2. (Color online) (a) Dependence of the long-lived spin coherence amplitude $\mathcal{A}_s$ on the carrier Larmor precession frequency for different values of τ_r/τ_s^T. (b), (c) Carrier spin coherence $S_z(t)$ normalized to $S_z(0)$ for two different values of τ_r/τ_s^T. The spin dynamics at zero magnetic field is shown by the dashed lines. The solid lines show $S_z(t)$ at finite magnetic field ($\omega\tau_r = 2.4$). The arrows show the corresponding amplitudes $\mathcal{A}_s(\omega/\gamma)$ for these conditions.

Figures 2(b) and 2(c) show the carrier spin coherence $S_z(t)$ calculated for fast ($\tau_r/\tau_s^T = 10$) and slow ($\tau_r/\tau_s^T = 0.01$) spin relaxation of the trion. The solid and dashed lines show $S_z(t)$ at zero and finite magnetic field, respectively. One can see from Fig. 2(b) that at $\tau_r/\tau_s^T = 10$, the amplitude of the long-lived spin coherence ($t \gg \tau_r$) in magnetic field coincides with the one at $B = 0$. In the graph, this corresponds to the coincidence of the dashed line (zero field) with the maxima of the oscillating solid line (finite field, $\omega/\gamma = 0.24$). In other words, the application of magnetic field here does not change the efficiency of spin coherence generation. This is, however, not the case for the smaller ratio of $\tau_r/\tau_s^T = 0.01$ ($\omega/\gamma = 240$). As one can see in Fig. 2(c), the dashed line at longer delays has considerably smaller amplitude than the maxima of the solid line $\mathcal{A}_s(0) \ll \mathcal{A}_s(240)$. This means that the amplitude of long-lived spin coherence $\mathcal{A}_s$ can be strongly increased by external magnetic fields. To conclude, even in the absence of spin relaxation in the trion, the application of an external magnetic field leads to appearance of long-lived spin polarization of the resident carriers.

4. Effect of spin precession in trion on spin coherence of resident carrier

Spin precession of the trion, characterized by the frequency Ω, also provides a mechanism for generating long-lived carrier spin coherence. It plays an important role in the case of the T^+ trion excited in p-doped structures,[36] where the trion spin corresponds to the electron one. In n-doped structures, although the in-plane hole g factor in quantum wells and in self-assembled quantum dots is rather small,[32–34] the spin precession of the hole in the T^- trion may become important in tilted magnetic fields.[35]

Allowing for $\Omega \neq 0$ results in the following expression for the amplitude of the long-lived spin coherence $\mathcal{A}_s$ [c.f. Eqs. (11) and (12)]:

$$\mathcal{A}_s = \left|S_z^a - S_z^{T,a}\xi\right| = \left|S_z^a(1+\xi)\right| \approx |S_{z,0}|\frac{(\Omega\tau_r)^2}{1+(\Omega\tau_r)^2}, \tag{13}$$

where in the latter equality we assume a trion spin relaxation time $\tau_s^T \gg \tau_r$ and neglect the resident carrier spin precession $\omega \ll \Omega$. It follows from Eq. (13) that the spin precession in the trion acts similar to the trion spin relaxation. Here, it does not matter whether the spin of the unpaired carrier in the trion was rotated by the magnetic field or flipped due to spin relaxation: in both cases, long-lived carrier spin polarization arises.

The situation becomes richer when spin precession of both resident carrier and trion occurs. Figure 3 shows the spin dynamics of T^- trion and resident electron [Fig. 3(a), n-type] and T^+ trion and resident hole [Fig. 3(b), p-type]. The black curves give the difference $S_z^T - S_z$, which corresponds to signals commonly measured in experiment [see also Eqs. (54) and (57) in Ref. 23]. It is clearly seen that at short delay times not exceeding the trion lifetime, the $S_z^T - S_z$ dynamics is additionally modulated by the trion Larmor frequency. For clarity, the spin dynamics of trions S_z^T is shown separately by the gray (red) lines. They decay relatively fast being limited by the trion recombination. The trion radiative lifetimes as well as spin relaxation times are taken the same in both Figs. 3(a) and 3(b): $T_R/\tau_r = 130$, $T_R/\tau_s^T = 13$, and $T_R/\tau_s = 2.6$. The carrier and trion Larmor precession frequencies are given in these figures. Here, T_R is the repetition period of excitation pulses and $\omega_R = 2\pi/T_R$. For commonly used mode-locked lasers with a repetition frequency of 75 MHz, $T_R = 13.3$ ns. Note that Fig. 3 is calculated for a single pump pulse and T_R is introduced here solely as a unit of time.

C. Spin accumulation induced by a train of pump pulses

In experiments on coherent spin dynamics, periodic trains of pump pulses are commonly used. When the spin relaxation time of the resident carrier is comparable or longer than the repetition period of the pump pulses, i.e., $\tau_s > T_R$, the cumulative contribution of multiple pump pulses results in the accumulation of the carrier spin polarization and its periodicity with the period T_R. In external magnetic fields applied in the Voigt geometry, this accumulated periodical polarization is reached for each precessing spin by relatively long trains of pump pulses: the decay of the spin polarization is then balanced by the pumping. As a result, the carrier spin after each repetition period $\boldsymbol{S}(T_R)$, given by Eq. (6), should be equal to the carrier spin right before the pump pulse arrival, which we denote by $\boldsymbol{S}^b$ (see Fig. 4). As before, instant pump pulse action is assumed. Then, $\boldsymbol{S}^b$ corresponds to the limit of carrier spin polarization at time delay approaching zero delay from negative side $t \to 0^-$. Using the connection between the carrier spins before and after the pump pulse [Eq. (1)], and assuming that the pump pulse is resonant with the trion transition, $\Phi = 0$, one immediately comes to the following

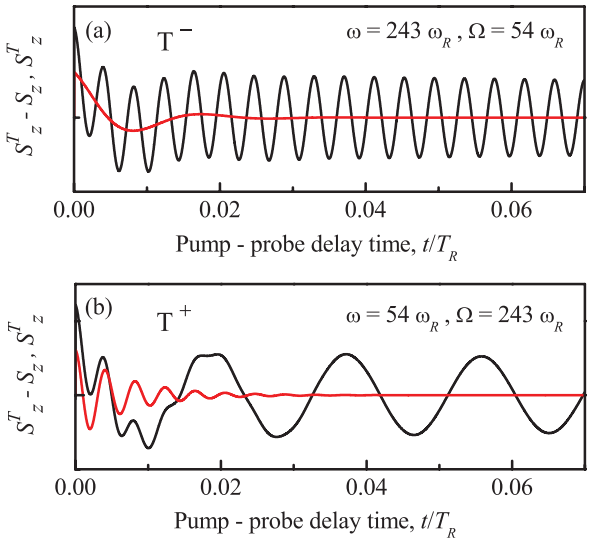

FIG. 3. (Color online) Spin dynamics of resident carriers and trions for (a) negatively charged trions T^-, n-type and (b) positively charged trions T^+, p-type. The black curves show the temporal evolution of $S_z^T - S_z$. The gray (red) curves give only the trion contribution to the signal S_z^T.

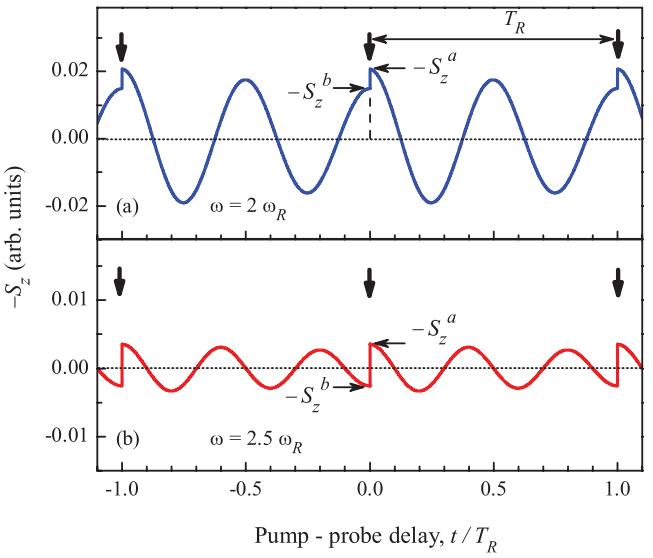

FIG. 4. (Color online) Dependencies of resident carrier spin polarization S_z on pump-probe delay for a carrier spin precession frequency, which is (a) commensurable with the pump repetition frequency $\omega = 2\omega_R$ and (b) not commensurable with this frequency $\omega = 2.5\omega_R$. Parameters of calculations are $\tau_s = 3T_R$, $\Theta = 0.1\pi$, $\tau_s^T \ll \tau_r$. Thick vertical arrows show the arrival times of the pump pulses. Phase ϕ of the oscillating polarization $-S_z$ is $\phi = 0$ in panel (a) and $\phi = \pi$ in panel (b).

expression for the carrier spin z component before pump pulse arrival:

$$S_z^b(\omega) = \pm\frac{1}{2}\frac{K}{1 + Qe^{-2T_R/\tau_s} - e^{-T_R/\tau_s}(1+Q)\cos(\omega T_R) - K}, \tag{14}$$

where the signs $\pm$ correspond to different polarizations of optical pumping and different types of resident carriers [cf. Eqs. (1)], and

$$K = \frac{(1-Q^2)e^{-T_R/\tau_s}}{2}\{(1+\xi_1)[Qe^{-T_R/\tau_s} - \cos(\omega T_R)] - \xi_2 \sin(\omega T_R)\}.$$

Equation (14) shows that the spin z component before the next pump pulse arrival S_z^b is a periodic function of magnetic field (see Fig. 5) with maxima of $|S_z^b|$ at frequencies ω satisfying the phase synchronization condition[5,14,37] (PSC)

$$\omega = N\omega_R = \frac{2\pi N}{T_R}, \quad N = 0,1,2,\ldots. \tag{15}$$

Here, $\omega_R = 2\pi/T_R$ is the repetition frequency of the pump pulses. Indeed, as one can see from time-resolved signals shown in Fig. 4, if the spin precession period of the resident carrier is commensurable with the pump pulse repetition period, then the spin coherence generated by the pump is always in phase with that from the previous pulse [see signal around zero time delay, Fig. 4(a)], and carrier spin polarization is accumulated. Otherwise, if the spin precession and pump repetition periods are not commensurable, the accumulation of spin polarization is not efficient, as seen from the comparison of the amplitudes in Figs. 4(a) and 4(b).

In general, the electron spin precession has a particular phase [see Eq. (11)], which we determine here as the difference $(\omega T_R - 2\pi N)$, where N is the largest integer satisfying the condition $(\omega T_R - 2\pi N) \geqslant 0$. The phase can be expressed as

$$\cos(\phi) = -S_z^b/\sqrt{(S_z^b)^2 + (S_y^b)^2},$$
$$\sin(\phi) = S_y^b/\sqrt{(S_z^b)^2 + (S_y^b)^2}. \tag{16}$$

Note that in Fig. 4 and further on in this paper we show for convenience the inverted signal $-S_z$ (in order to have positive signals at zero delay after pulse pump arrival $t \to 0^+$ for σ^+ pumping). This sign change does not affect the obtained results, but is more suitable for their graphic presentation.

It is worth to mention that Eq. (14) is valid both for a single dot and for an ensemble of identical dots with the same spin precession frequencies. For an ensemble of resident carriers with different spin precession frequencies ω, Eq. (14) should be averaged over their distribution[38] [see Sec. III D and Eq. (28)].

Figure 5 shows S_z^b calculated after Eq. (14) for different pump pulse areas Θ in the case of fast trion spin relaxation. As the x axis scale in Fig. 5, we take the ratio of spin precession frequency ω and ω_R, which represents the magnetic field dependence of S_z^b as $\omega \propto B$. Integer numbers on the x axis correspond to magnetic fields, for which the spin precession frequency satisfies the PSC of Eq. (15). At these magnetic fields, the amplitude of the resident carrier spin polarization $-S_z^b$ increases resonantly, evidencing favorable conditions for spin accumulation [see Fig. 5(a)]. It is obvious that the accumulation efficiency is controlled by the factor τ_s/T_R, as the accumulation occurs only when the spin relaxation time of the resident carrier τ_s exceeds considerably the repetition period of the pump pulses. This is confirmed by the

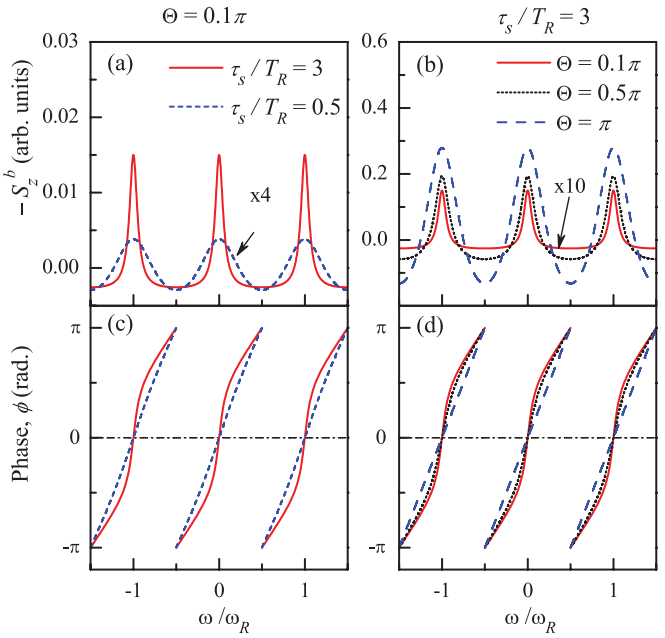

FIG. 5. (Color online) Dependence of the resident carrier spin polarization S_z^b and its phase on magnetic field expressed by $\omega/\omega_R = g\mu_B B/(\hbar\omega_R)$. $\tau_s^T \ll \tau_r$. Data are shown for zero time delay (right before the pump pulse arrival, $t \to 0^-$), calculated for different ratios τ_s/T_R at $\Theta = 0.1\pi$ (a), (c) and for different pump pulse areas Θ at $\tau_s/T_R = 3$ (b), (d).

calculations shown in Fig. 5(a). For a fixed value of τ_s/T_R, an increase of the pump pulse area results in a broadening of the peaks [see Fig. 5(b)]. The phases of the signals from Figs. 5(a) and 5(b) are shown in Figs. 5(c) and 5(d), respectively. One clearly sees that the zeros of the phase correspond to maxima of spin polarization $-S_z^b$, and the values $\phi = \pm\pi$ correspond to its minima.

One should note that the magnitude of the accumulated spin polarization, as well as the width of the resonant peaks in the magnetic field dependence of $-S_z^b$, are determined not only by the pump pulse power and the carrier spin relaxation time, but also by the mechanism of long-lived spin coherence generation and the spin dephasing time. We present the analysis of these effects in the following sections.

III. RESONANT SPIN AMPLIFICATION

We begin with the classical expression for carrier spin polarization under RSA conditions.[5,37] The underlying assumptions are the following: (i) only resident carrier spin polarization is considered, and (ii) it is supposed that each pump pulse generates only a z component of spin polarization, the magnitude of which is S_0. All nonadditive effects of the pump pulse[28] are disregarded. After single pump pulse excitation, the carrier spin dynamics are described by a decaying cosine function periodic with the Larmor precession frequency ω and decay with time τ_s. The effect of a long train of pump pulses on the carrier spin polarization can be calculated as

$$S_z(\omega,t) = \sum_{k=0}^{\infty} S_0 e^{-(t+kT_R)/\tau_s} \cos[\omega(t+kT_R)], \qquad (17)$$

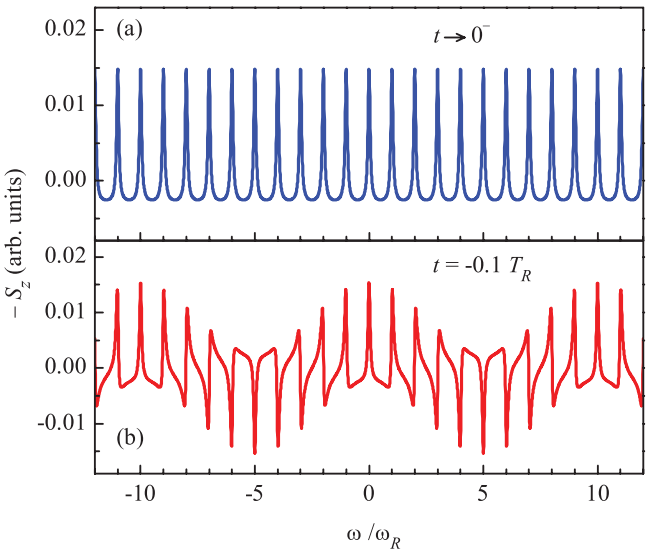

FIG. 6. (Color online) Carrier spin polarization S_z as function of magnetic field ($\omega \propto B$) at two different pump-probe delays denoted in each panel. $t \to 0^-$ means that the signal is calculated for very small negative delay, just before the pump pulse arrival. Parameters of calculations: $\tau_s = 3T_R$, $\Theta = 0.1\pi$, $\tau_s^T \ll \tau_r$.

where t is the pump-probe delay and $k = 0,1,2,\ldots$. This equation can be rewritten[37,38] as

$$S_z(\omega,t) = \frac{S_0}{2} e^{-t/\tau_s} \times \frac{e^{-T_R/\tau_s}\cos(\omega t) - \cos[\omega(t+T_R)]}{\cosh(T_R/\tau_s) - \cos(\omega T_R)}. \qquad (18)$$

It follows from Eq. (18) that for sufficiently long decay times $\tau_s \gtrsim T_R$, the carrier spin has sharp resonances as a function of magnetic field. This corresponds to the solid line in Fig. 5(a) and gives the RSA signals presented in Fig. 6. The peak positions at zero pump-probe delay correspond to spin precession frequencies, which are commensurable with the pump repetition frequency $\omega_R = 2\pi/T_R$. The expression (18) near commensurable frequency ($|\omega T_R - 2\pi N| \ll 1$) and at a zero time delay can be written as

$$S_z^b \sim \frac{1}{(\omega T_R - 2\pi N)^2 + (T_R/\tau_s)^2}. \qquad (19)$$

Here, we assume that $T_R/\tau_s \ll 1$. The peak width is determined by the relaxation time of the electron spin polarization. Note that for the spin ensemble, the time τ_s should be changed to the dephasing time T_2^* provided that $T_2^* \gtrsim T_R$ (see Sec. III D).[39] This allows one to measure spin relaxation and spin dephasing times exceeding T_R, i.e., for conditions where direct determination by time-resolved methods becomes inapplicable. Equations (18) and (19) describe a number of experiments well (see, e.g., Refs. 5, 37, 40, and 41), and facilitate evaluation of carrier g factors and spin dephasing times.[39]

However, one sees that the spin polarization in Eqs. (18) and (19) increases to infinity if τ_s becomes larger and larger. Moreover, such an approach disregards completely the spin dynamics of trions and the specifics of carrier spin dephasing in external magnetic fields. This case requires a special treatment.

There are also experiments that reveal a complicated shape of RSA spectra or a complete absence of RSA despite very long spin relaxation times, which can not be described by this simple model.[36,42,43] The general analysis required for such cases is presented below.

A. Fast spin relaxation in trion

If the spin relaxation of the unpaired carrier in the trion is fast, $\tau_s^T \ll \tau_r$, the trion spin dynamics does not affect the spin polarization of the resident carriers (see Sec. II B 2). In this case, the carrier polarization induced by the pump pulse is not compensated by the carriers left after trion recombination, as these carriers are unpolarized. Then, $\xi = 0$ and the parameter K in Eq. (14) has the simple form[14,23]

$$K = \frac{(1-Q^2)e^{-T_R/\tau_s}}{2}[Qe^{-T_R/\tau_s} - \cos(\omega T_R)]. \qquad (20)$$

The detailed analysis of Eqs. (14) and (20) for this case is given in Refs. 14 and 23. If, moreover, the pump pulse area Θ is small, so that $1-Q \ll 1$, Eq. (14) together with Eq. (20) go over into the classical expression of Eq. (18) for the carrier spin polarization under RSA conditions.

It follows that for frequencies near the phase-synchronization condition of Eq. (15), the spin z component of the resident carrier can be recast as[23]

$$S_z^b \sim \frac{1}{(\omega T_R - 2\pi N)^2 + [T_R/\tau_s + (1-Q)]^2}, \qquad (21)$$

where we assume that $T_R/\tau_s \ll 1$, $1-Q \ll 1$, and $|\omega T_R - 2\pi N| \ll 1$. One sees from Eq. (21) that the RSA peak width is determined by T_R/τ_s or $1-Q$, whichever is larger.

Figure 6 shows RSA signals calculated for a small pump power $\Theta = 0.1\pi$ at two different delays. The shape of the RSA signal at large negative delay ($t = -0.1T_R$) differs from the one at very small negative delay due to the different phases of the spin precession.

An increase of the pump pulse area results in broadening of the RSA peaks, as was already shown in Fig. 5(b). For increasing pump pulse area, the RSA peaks are no longer Lorentzians and, therefore, S_z^b can not be described by Eq. (21). The spin polarization for $\Theta = \pi$ and $\tau_s/T_R = 3$ shown in Fig. 5(b) looks similar to the one for $\Theta = 0.1\pi$ and $\tau_s/T_R = 0.5$ in Fig. 5(a). Hence, under strong excitation, the dependence of carrier spin polarization on magnetic field becomes cosinelike due to saturation effects. In this case, it is not possible to extract the carrier spin relaxation or the dephasing times from the width of RSA peaks.

B. Slow spin relaxation in trion: Effect of trion spin dynamics

Let us now turn to the general case in which the trion spin relaxation time can be comparable or even longer than its recombination time. It is instructive to start from the situation in which $\tau_s^T \gg \tau_r$ and long-lived spin coherence appears only due to carrier or trion spin precession about the magnetic field. Clearly, the peaks in the $S_z^b(\omega)$ dependence are suppressed for $\omega\tau_r, \Omega\tau_r \ll 1$ due to inefficient spin generation, and they increase significantly with an increase of magnetic field. This is illustrated in Fig. 7, where the calculated RSA signals are shown for $\tau_s^T = 30\tau_r$. Note that such unusual RSA spectra with suppression of the peak amplitudes in weak magnetic fields have been observed experimentally in both n-type and p-type QWs.[22,36,42,44]

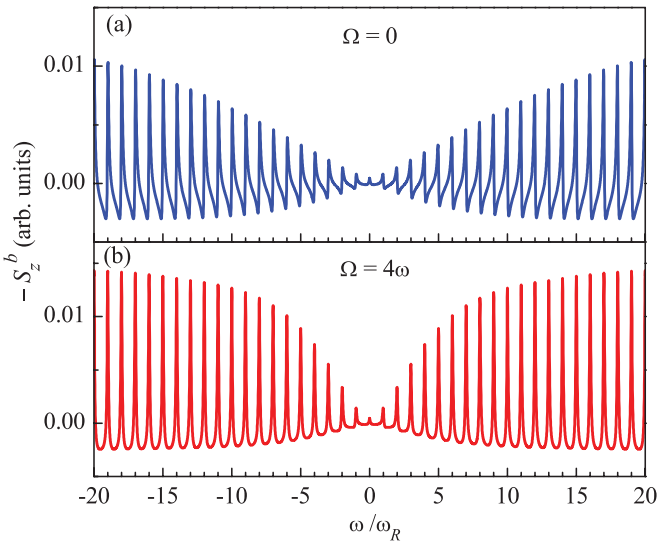

FIG. 7. (Color online) Impact of slow spin relaxation of the unpaired spin in the trion: RSA signals at zero delay ($t \to 0^-$) without ($\Omega = 0$) and with ($\Omega = 4\omega$) trion spin precession [panels (a) and (b), respectively]. Parameters of calculations: $\tau_s^T = 30\tau_r$, $\tau_r = 0.01T_R$, $\tau_s = 3T_R$, and $\omega\tau_r = 4.4$ at $B = 1$ T and $\Theta = 0.1\pi$.

Figure 7(a) shows the signal calculated in absence of trion spin precession ($\Omega = 0$) shortly before the pump pulse arrival. The peak amplitude at zero magnetic field ($\omega = 0$) is given by the ratio τ_r and τ_s^T and goes to zero for infinite τ_s^T. The increase of peak amplitudes with increasing magnetic field depends on ξ and, therefore, on the ratio ω/γ, similar to the amplitude dependencies in Fig. 2. The peak shapes at small negative delay differ from being Lorentzian [see for comparison Eq. (21) and Figs. 5(a), 5(b), and 6(a)] because the spin left behind after trion recombination changes the phase of the carrier spin precession.[9]

It is worth to stress that we can use the same system of Equations (5) to describe the spin dynamics in n-type (resident electron and T^- trion) and p-type (resident hole and T^+ trion) structures. Figure 7(a) illustrates the situation that can be realized for n-type QWs,[31,42] in which trion spin precession is absent. Figure 7(b) shows the RSA signal with a trion spin precession frequency $\Omega = 4\omega$, which may correspond to the T^+ trion case in p-type QWs.[36,44] The analysis shows that small Ω, i.e., $\Omega \leqslant \omega$, leads to no significant changes of the RSA signal shape as compared with one in Fig. 7(b). A fast precession of the trion spin results in a faster appearance of long-lived spin coherence with increasing magnetic field [compare Figs. 7(a) and 7(b)].

C. Effect of spin relaxation anisotropy

To make our analysis of RSA complete, we briefly discuss here another effect, which is relevant for weak magnetic fields. It addresses the situation in which the carrier spin relaxation or the dephasing times are anisotropic. spin relaxation anisotropy is an inherent feature of semiconductor quantum wells.[45–49] For simplicity, we consider the case in which the z and y spin components of the resident carriers relax at different time

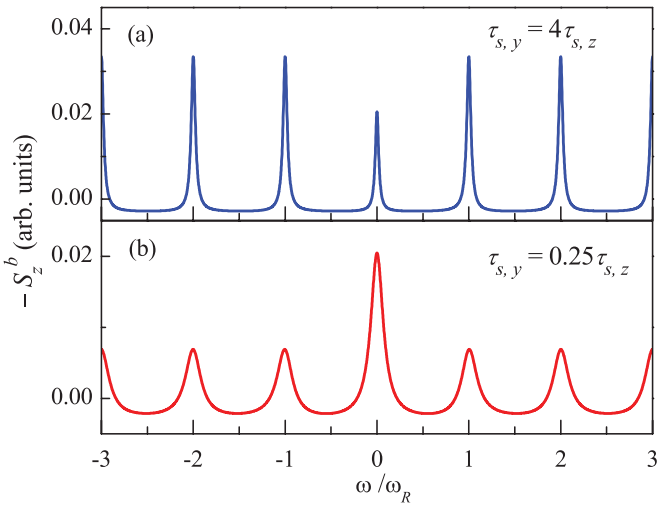

FIG. 8. (Color online) Effect of an anisotropy of the carrier spin relaxation times. The electron spin z component right before pump pulse arrival $t \to 0^-$ is calculated as function of magnetic field after Eq. (22). $\tau_{s,z} = 4T_R$. $\tau_s^T \ll \tau_r$.

constants $\tau_{s,z}$ and $\tau_{s,y}$, respectively. Provided that the long-lived carrier spin coherence is excited by the train of weak pump pulses, the dependence of the carrier spin z component on the precession frequency is given by[38]

$$S_z^b(\omega) \sim \frac{\mathcal{C}(\tilde{\omega}T_R) - e^{-T_R/\tau_s}}{\cosh(T_R/\tau_s) - \cos(\tilde{\omega}T_R)}, \tag{22}$$

where

$$\frac{1}{\tau_s} = \frac{1}{2}\left(\frac{1}{\tau_{s,z}} + \frac{1}{\tau_{s,y}}\right), \quad \tilde{\omega} = \sqrt{\omega^2 - \frac{1}{4}\left(\frac{1}{\tau_{s,z}} - \frac{1}{\tau_{s,y}}\right)^2} \tag{23}$$

and

$$\mathcal{C}(\tilde{\omega}T_R) = \cos(\tilde{\omega}T_R) - \frac{1}{2\tilde{\omega}}\left(\frac{1}{\tau_{s,z}} - \frac{1}{\tau_{s,y}}\right)\sin(\tilde{\omega}T_R).$$

The dependence of carrier spin polarization $-S_z^b$ on magnetic field is shown in Fig. 8 for two cases of anisotropic carrier spin relaxation: (a) $\tau_{s,y} = 4\tau_{s,z}$ and (b) $\tau_{s,y} = 0.25\tau_{s,z}$. The amplitudes of all maxima except the one at zero field are the same because they are determined by the effective spin relaxation time τ_s defined by Eq. (23). The amplitude of the zero-field peak is different from the other peaks. If $\tau_{s,y} > \tau_{s,z}$, it is smaller as compared with the others. The carrier spin relaxation in absence of a magnetic field is governed solely by $\tau_{s,z}$ and is faster than at finite magnetic fields, so that accumulation of carrier spin polarization is weaker at $B = 0$. In the opposite case of $\tau_{s,y} < \tau_{s,z}$ the zero-field peak is higher because the lifetime of the spin z component is longer in absence of magnetic field so that spin accumulation is more efficient.[50]

D. Spin decoherence and dephasing

The spin relaxation time of localized carriers can be extremely long reaching up to microseconds for electrons in QDs, for example.[51] This is related with quenching of the orbital motion and the corresponding suppression of spin relaxation mechanisms contributed by spin-orbit coupling.[52,53] The coherence time of an individual spin is typically much longer compared with the spin dephasing time of an inhomogeneous spin ensemble. The inhomogeneity, which leads to a spread of carrier spin precession frequencies, results in spin dephasing characterized by the T_2^* dephasing time. This time measured, e.g., from the decay of spin beats in external magnetic field is in the few nanoseconds range for QD ensembles[14,15,54] and in the tens of nanoseconds range for QWs containing diluted carrier gases.[9,22,30,40]

One of the main origins for the inhomogeneity of a spin ensemble is related to the g-factor spread of localized carriers. For electrons, the g-factor variation can arise from changes of the effective band gap for different localization sites.[14,55,56] For localized holes, the variations are mainly related to changes in the mixing of heavy- and light-hole states.[57] The spread of g factors in a spin ensemble Δg is translated into a spread of spin precession frequencies $\Delta\omega_g$ and, therefore, results in a spin dephasing rate[38,40]

$$\frac{1}{T_{2,\Delta g}^*} \sim \frac{\Delta g \mu_B B}{\hbar} \equiv \Delta\omega_g, \tag{24}$$

which is accelerated with increasing magnetic field.

Another origin of spin dephasing typical for electrons is related to random nuclear fields in the quantum dots.[58] Each localized electron is subject to a hyperfine field of a particular nuclear spin fluctuation $\boldsymbol{B}_\mathrm{n}$ and, therefore, precesses about this field at a frequency ω_n. These fluctuations are different for different localization sites, causing dephasing of the electron spin ensemble. The dephasing rate can be estimated by the root mean square of the electron spin precession frequency in the field of frozen nuclear fluctuations[58]:

$$\frac{1}{T_{2,\mathrm{n}}^*} \sim \sqrt{\langle\omega_\mathrm{n}^2\rangle}. \tag{25}$$

Assuming a normal distribution of $\boldsymbol{B}_\mathrm{n}$, Eq. (25) can be rewritten as

$$\frac{1}{T_{2,\mathrm{n}}^*} \sim \frac{g\mu_B\Delta_B}{\hbar} \equiv \Delta\omega_\mathrm{n}, \tag{26}$$

where Δ_B is the dispersion of the nuclear spin fluctuation distribution.[58]

Estimates show that $T_{2,\mathrm{n}}^*$ is on the order of several nanoseconds for GaAs quantum dots.[58,59] Hence, in weak magnetic fields [e.g., $B \lesssim 0.3$ T for $g = 0.5$ and $\Delta g = 0.005$ (Ref. 43)], the spin beat decay for resident electrons is determined by the hyperfine interaction, and in higher fields the dephasing is caused by the spread of g factors.[60]

In quantum wells with a diluted electron gas, the electron localization on well width fluctuations is considerably weaker compared to the QD case. As a result, Δg is smaller and the hyperfine interaction is weaker. Therefore, the spin dephasing times can reach $\sim$ 30–50 ns in weak magnetic fields and at low temperatures.[9,22] In the following, the effect of a spin precession frequency spread on RSA signals is analyzed.

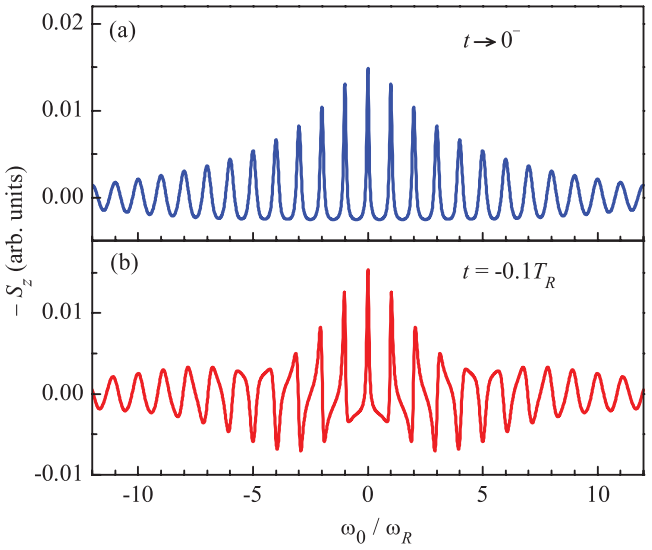

FIG. 9. (Color online) Dependencies of carrier spin polarization S_z on magnetic field at two different pump-probe delays t given in each panel and short trion spin relaxation time $\tau_s^T \ll \tau_r$. A frequency spread $\Delta\omega_g = 0.02\omega_0$, corresponding to 2% dispersion of the carrier g factor, is assumed in the calculations. The dependence on magnetic field is given by $\omega_0/\omega_R = g_0\mu_B B/(\hbar\omega_R)$.

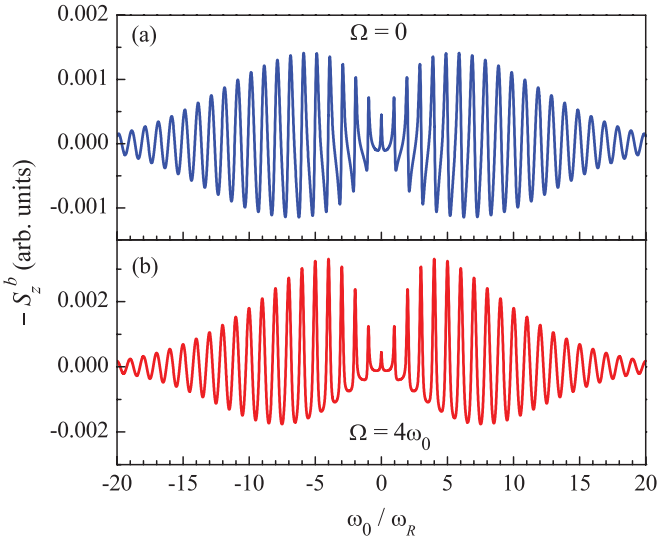

FIG. 10. (Color online) Effect of slow trion spin relaxation. RSA signals at zero delay ($t \to 0^-$) without [(a) $\Omega = 0$] and with [(b) $\Omega = 4\omega_0$] trion spin precession are shown. The signals are calculated assuming a spin precession frequency spread $\Delta\omega = 0.02\omega_0$ of the resident carrier. The parameters in the calculations are $\tau_s^T = 30\tau_r$, $\tau_r = 0.01T_R$, $\tau_s = 3T_R$, and $\omega_0\tau_r = 4.4$ at $B = 1$ T and $\Theta = 0.1\pi$.

1. Spread of g factors

For a more realistic approach, we need to take into account the precession frequency spread $\Delta\omega$ in the spin ensemble. Here, for distinctness, we consider only the frequency spread caused by Δg (the spread related with the nuclear spin fluctuations is considered below). For ensemble of carrier spins with a spread of g factors Δg, the spread of Larmor precession frequencies $\Delta\omega_g$ is proportional to the magnetic field:

$$\Delta\omega_g(B) = \Delta g\mu_B B/\hbar. \tag{27}$$

To model the ensemble RSA signal, one has to sum the contributions of the individual spins[38] over the g-factor distribution function:

$$\rho(g) = \frac{1}{\sqrt{2\pi}\Delta g}\exp\left[\frac{-(g-g_0)^2}{2(\Delta g)^2}\right], \tag{28}$$

where g_0 is the average g-factor value in the spin ensemble, resulting in an average Larmor frequency: $\omega_0 = g_0\mu_B B/\hbar$.

RSA spectra calculated by means of Eqs. (14) and (28) for short trion spin relaxation are presented in Fig. 9 for two negative time delays. Here, the magnetic field is shown in terms of ω_0/ω_R. An increase of magnetic field leads to broadening of the RSA resonances and decrease of their amplitudes. This reflects the acceleration of the spin dephasing rate $1/T_2^* \sim B$, in accordance with Eq. (24).

Figures 10(a) and 10(b) show RSA signals for long trion spin relaxation $\tau_s^T = 30\tau_r$ with and without spin precession in the trion. An ensemble spread of $\Delta\omega_g = 0.02\omega_0$ results in a broadening of the RSA peaks and a decrease of their amplitudes with increasing magnetic field, similar to Fig. 9. This results in the characteristic batlike shape of the RSA signal[22,36,42,44] (compare with Fig. 7) where the spin dephasing was absent, $\Delta\omega_g = 0$. Accounting for the spread of Ω does not change the signals significantly.

Figure 10(a) corresponds to a situation that is obtained for resident electrons oriented by excitation of the T^- trion in n-type (In,Ga)As/GaAs QWs.[22,42] In such structures, the in-plane hole g factor is small compared with the electron g factor and, consequently, $\Omega \ll \omega$, so that the spin precession of the T^- trion can be neglected.

Figure 10(b) corresponds to the long-lived hole spin orientation for excitation of the T^+ trion in p-type GaAs/(Al,Ga)As QWs.[36] For the T^+ trion, the ratio Ω and ω is opposite, i.e., $\Omega \gg \omega$. In Ref. 36, $\Omega = 4.5\omega$ and the spin precession in trion affects the RSA signal.

The results of the calculations shown in Figs. 10(a) and 10(b) are in good agreement with available experimental data for quantum well structures.[22,36,42] All calculations were done for a small pulse area $\Theta = 0.1\pi$. The analysis of the case of high pump power, which results in saturation effects, shows that an increase of the pump power results in an increase of the signal amplitude and broadening of all peaks, similar to the case discussed in Sec. III A (see also Fig. 5). The batlike shape of the RSA signal envelope is conserved even for $\Theta = \pi$ pump pulses.

2. Nuclear field fluctuations and resonant spin amplification in weak magnetic fields

Interaction of the nuclear spins with hole spins is weak and in many cases can be neglected. At the same time, for localized electrons, the hyperfine interaction with the nuclei can considerably contribute to the spin dynamics. Therefore, in this section, we will focus on n-type structures containing resident electrons.

In weak magnetic fields, the electron spin dephasing time related to the spread of g-factor values [Eq. (24)], proportional to $1/B$, becomes very long, and nuclear field fluctuations play an important role. The hyperfine fields acting on the electrons due to these nuclear fluctuations can be as large as $B_n \sim 0.5$ mT for GaAs QWs (Ref. 30) and an order of magnitude larger in (In,Ga)As QDs.[61]

For $B \gtrsim B_n$, the only important component of the nuclear field fluctuation is the one parallel to the external field $\boldsymbol{B}$. It results in a spread of Larmor precession frequencies, damping of the spin beats, and broadening of the RSA peaks, provided $B_n > |\Delta g/g|B$.

The situation becomes different in weak magnetic fields $B < B_n$. In this case, all components of the nuclear fluctuation field become important. For illustration, we consider a homogeneous electron spin ensemble ($\Delta g = 0$) in a magnetic field, which is the sum of the external magnetic field $\boldsymbol{B}$ and the fluctuation field $\boldsymbol{B}_n$. For simplicity, we consider the regime of fast spin relaxation in the trion ($\tau_s^T \ll \tau_r$). To model the dynamics of the electron spin ensemble, one can assume a normal distribution of $\boldsymbol{B}_n$:

$$\rho_n(\boldsymbol{B}_n) = \frac{1}{(\sqrt{2\pi}\Delta_B)^3} \exp\left(-\frac{\boldsymbol{B}_n{}^2}{2(\Delta_B)^2}\right), \tag{29}$$

where Δ_B is the isotropic dispersion of the nuclear fluctuation field distribution ($\Delta_{B,x} = \Delta_{B,y} = \Delta_{B,z}$). The spread of the Larmor precession frequencies $\Delta\omega_n$ does not depend on the external magnetic field:

$$\Delta\omega_n = g\mu_B\Delta_B/\hbar. \tag{30}$$

The average Larmor frequency of the spin ensemble in this case is equal to the spin precession frequency in an external magnetic field without nuclear fluctuations: $\omega_0 = g\mu_B B/\hbar$.

Figure 11 shows RSA signals at zero time delay ($t \to 0^-$) averaged over B_n for different Δ_B values. One sees that, indeed, an increase of the frequency spread $\Delta\omega_n$ leads to an increase of the dephasing rate evidenced via broadening of the RSA peaks. For weak magnetic fields $B < \Delta_B$, the y component of the nuclear fluctuation field $B_{n,y}$, which is perpendicular to S_z and to the external field, can additionally destroy the long-lived carrier spin polarization. This is manifested in an additional broadening and a decrease of the amplitude of the zeroth RSA peak (compared to the ± 1 peaks), as is clearly seen in Figs. 11(a) and 11(b). The enhancement of S_z in the vicinity of zero field for large fluctuations [see Fig. 11(c)] is due to the fact that the z component of the spin polarization can not be destroyed by a parallel component of the nuclear fluctuation field $B_{n,z}$.

E. Analysis of RSA signals and evaluation of spin dephasing times and g factors

To conclude our analysis of RSA, we emphasize that in spite of the possibly complex shape of RSA signals, especially in case of a long spin relaxation in the trion, the analysis allows one to obtain various parameters with high accuracy. This is due to the fact that these parameters are responsible for different features in the RSA spectrum:

(i) The g factor of the resident carriers gives the magnetic field positions of the RSA peaks.

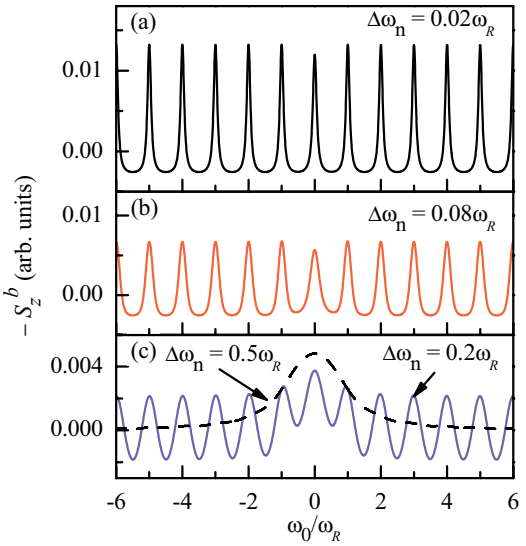

FIG. 11. (Color online) RSA signals at zero pump-probe delay $t \to 0^-$, calculated for different spreads of the nuclei fluctuation field Δ_B. The frequency spreads ($\Delta\omega_n \sim \Delta_B$) are given in each panel. $\Theta = 0.1\pi$, $\Delta g = 0$, and $\tau_s^T \ll \tau_r$.

(ii) The g-factor spread Δg determines the amplitude decrease of the RSA peaks with increasing magnetic field.

(iii) The spin relaxation and dephasing time τ_s is related to the RSA peak widths.[62]

(iv) The ratio of spin relaxation time τ_s^T and radiative lifetime τ_r of the trion determines the possible increase of RSA peak amplitudes with increasing magnetic field. If τ_r is obtained from an independent time-resolved measurement, then τ_s^T can be extracted from fitting the RSA spectrum.

(v) For long spin relaxation in the trion (when the RSA signal has a bat-like shape), the symmetry of the RSA peaks at small negative pump-probe delay can indicate the fact that the trion g factor is larger than that of the resident carrier ($|g_T| \gg |g|$). However, the value of the trion g factor should be obtained from another experiment.

(vi) Finally, the amplitude and the width of the zero-field RSA peak can contain information on the anisotropy of the spin relaxation of delocalized carriers and the nuclear effects for localized carriers.

The spin dynamics parameters considered above can be extracted only for sufficiently homogeneous ensembles and at weak excitation powers (small pump pulse areas), which is typical for semiconductor QWs.

It is worth to mention that there are other generation mechanisms of long-lived spin coherence for nonresonant optical excitation.[9,22,44] In this case, the RSA signal can change its shape dramatically. However, a detailed analysis allows one to identify the generation and relaxation mechanisms of carrier spin polarization and obtain the corresponding quantitative information about relaxation processes.

IV. MODE LOCKING OF CARRIER SPIN COHERENCES

Now, we turn to strongly inhomogeneous spin systems, for which the spread of the spin precession frequencies is so large

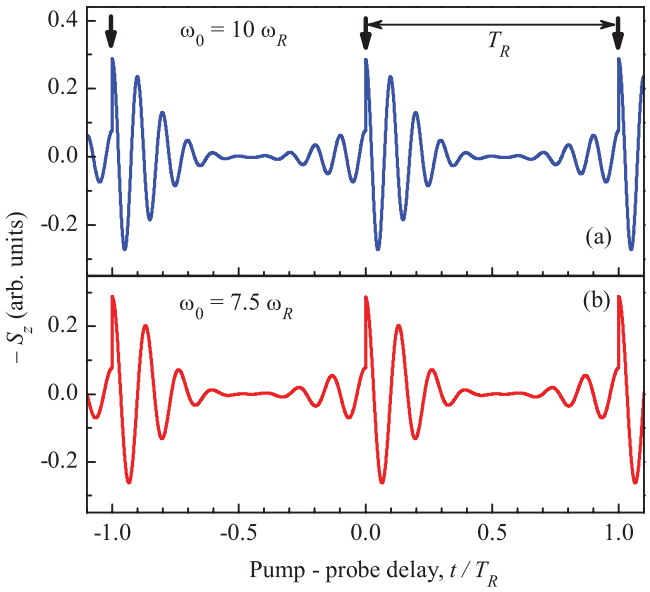

FIG. 12. (Color online) Carrier spin polarization as a function of pump-probe delay for precession frequencies which (a) satisfy the PSC of Eq. (15) and (b) do not satisfy it. The frequency spread is $\Delta\omega = \omega_R$, $\Theta = \pi$, and $\tau_s^T \ll \tau_r$. Thick vertical arrows indicate the arrival times of the pump pulses.

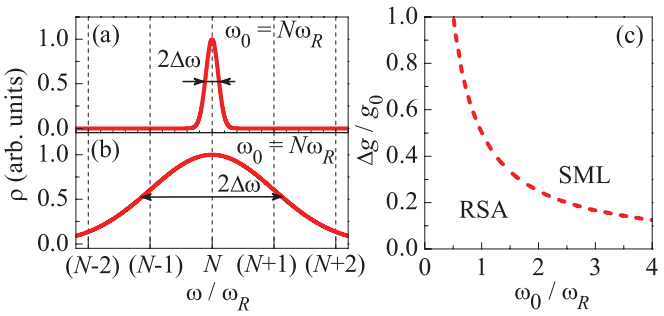

FIG. 13. (Color online) Larmor frequency distribution function (multiplied for convenience by $\sqrt{2\pi}\Delta\omega$) of a spin ensemble for RSA (a) and SML (b) conditions. (c) Parameter diagram showing schematically the regimes where RSA and SML occur, see text for details.

that

$$T_2^* < T_R. \tag{31}$$

Still, the spin relaxation time of the resident carrier is assumed to exceed by far the repetition period $\tau_s \gg T_R$. In this case, the ensemble spin polarization generated by a pump pulse decays within the time T_2^*, i.e., disappears before the next pump pulse arrival. Figure 12 presents model calculations, which show the dynamics of the carrier spin polarization excited by a train of the pump pulses. Indeed, the polarization decays quite rapidly after the pump pulses, but thereafter reemerges at negative delays $-T_2^* \lesssim t < 0$. Such a behavior has been explained as a synchronization of the electron spin precession frequencies by the periodic train of pump pulses.[14,20]

If the condition (31) is fulfilled, the pump pulse excites a broad distribution of spin precession frequencies, among which there are several frequencies satisfying the phase synchronization condition of Eq. (15). The carrier spins with such precession frequencies are excited much more efficiently, i.e., accumulate more spin polarization than the other ones. As a result, the main contribution to the signal is given by the commensurable spin beat frequencies. In other words, the spins satisfying the PSC become resonantly amplified, while others are not, and the synchronized spins contribute mostly to the experimentally measured signal of carrier spin polarization.

This phenomenon was termed "mode locking" by analogy with laser physics, where the generation is only possible for certain modes, the frequencies of which are equal to the cavity mode frequencies. By contrast with the lasers, where special techniques are employed to make synchronized modes coherent, for the spin mode locking, the modes with commensurable Larmor frequencies are always excited in phase by the pump pulses. Corresponding behavior of the spin signals has been observed in ensemble of n-type singly charged (In,Ga)As QDs.[14,20,21]

The calculations shown in Fig. 12 are carried out by means of averaging single electron spin dynamics Eq. (14) taking into account Eq. (30) for the spread of spin precession frequencies. We assume, for simplicity, that the trion spin relaxation is fast, $\tau_s^T \ll \tau_r$, and the spread of the carrier spin precession frequencies $\Delta\omega = \omega_R$ does not depend on the magnetic field strength.

Let us have a closer look on the signals in Fig. 12. It is remarkable that the phase of the spin beats before the next pump pulse arrival is fixed for any magnetic field. The average precession frequency of spin ensemble ω_0 satisfies the PSC in Fig. 12(a), while it does not in Fig. 12(b). The phase, however, in both cases is exactly the same and it also coincides with the one after the pump pulse $\phi = 0$. This is in strong contrast with the regime of weak dephasing ($T_2^* \gtrsim T_R$) [see Fig. 5(c)] and can be considered as the principal difference of the SML and RSA regimes of carrier spin accumulation. Note that the regime of weak dephasing is similar to the dynamics of a single spin presented in Figs. 4 and 5. It is worth to mention that the ratio of the signal amplitudes at negative and positive delays depends strongly on the generation efficiency and conservation of spin polarization, i.e., on the pump pulse area, the trion spin relaxation, and the ratio of carrier spin relaxation time τ_s to T_R.[14,20]

V. RSA VERSUS MODE LOCKING

In this section, we discuss how one can distinguish the RSA and SML regimes and what parameters are responsible for separating these regimes. This separation is based on the common basic mechanism of the RSA and SML effects, which is the accumulation of carrier spin polarization under periodic pump pulse excitation. The key difference between the regimes is the ratio of the Larmor frequency broadening to the repetition frequency of the pump pulses: $\Delta\omega/\omega_R$. This is schematically illustrated in Figs. 13(a) and 13(b) by the frequency spectrum of the spin ensemble in a finite magnetic field. Here, few PSC modes satisfying Eq. (15) from $(N-2)\omega_R$ to $(N+2)\omega_R$ are indicated by the dashed vertical lines.

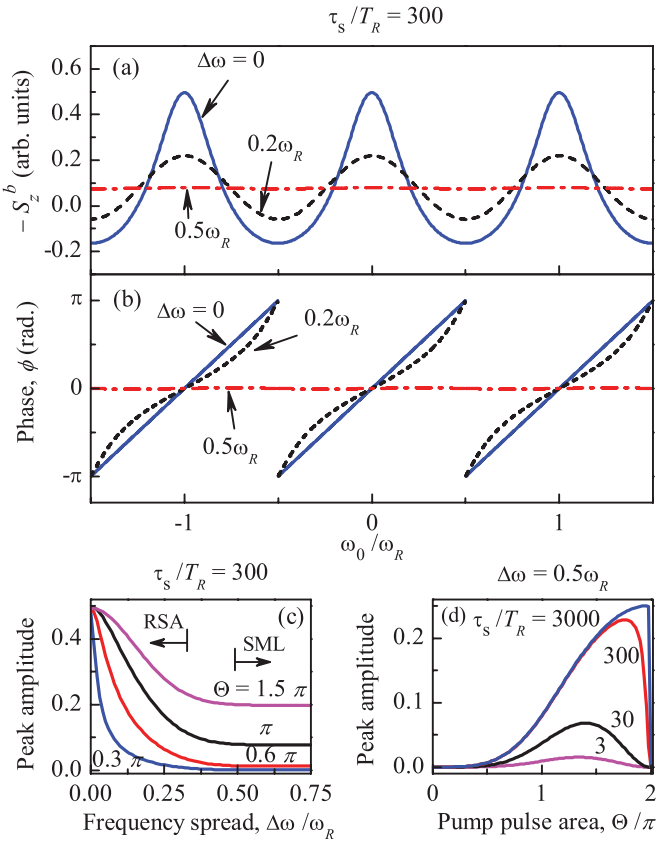

FIG. 14. (Color online) Magnetic field dependencies [in terms of $\omega_0(B)/\omega_R$] of (a) the carrier spin polarization amplitude $-S_z^b$ and (b) the signal phase at zero delay ($t \to 0^-$) calculated for three different Larmor frequency spreads. Dependencies of the spin polarization amplitude for PSC modes, i.e., for integer values of $\omega_0(B)/\omega_R$ (c) on the frequency spread for different pump pulse areas, at $\tau_s/T_R = 300$, and (d) on the pump pulse area for various τ_s/T_R for a precession frequency spread $\Delta\omega = 0.5\omega_R$. $\tau_s^T \ll \tau_r$.

In the RSA regime, $\Delta\omega \ll \omega_R$ and only one PSC mode (or even none) can fall into the distribution of Larmor frequencies. When the PSC mode coincides with the distribution maximum, as it is shown in Fig. 13(a), one obtains a peak in the RSA spectrum. And, when the overlap between the mode and the distribution is absent, the RSA spectrum has minimum.

For the SML regime, involvement of at least two PSC modes is necessary. Therefore, the condition for this regime is $\Delta\omega \gtrsim \omega_R$ [see Fig. 13(b)]. The calculations given in this section show that in fact the transition to the SML regime happens already for $\Delta\omega \gtrsim 0.5\omega_R$, when the tails of the Larmor frequency distribution overlap with more than one PSC mode.

Deeper insight in the separation between the RSA and SML regimes is collected below in Figs. 14, 15, and 16. Here, the carrier spin polarization amplitude S_z^b and the signal phase at zero delay ($t \to 0^-$) are analyzed as functions of magnetic field, time delay, Larmor frequency spread, and pump pulse area. We also consider the effect of resident carrier spin relaxation taking it into account via the parameter τ_s/T_R. For most figures, a pump pulse area $\Theta = \pi$ is chosen as it provides efficient spin accumulation. Let us go step by step through this data set.

First, for demonstration purposes, we assume again that a spread of the carrier spin precession frequencies is $\Delta\omega = \omega_R$, and it does not depend on magnetic field. For n-type structures, this corresponds to the case when the $\Delta\omega$ of the resident electrons is dominated by the random fields of the nuclear spin fluctuations: $\Delta\omega_n \propto B_{n,x}$. For $B > B_n$, only the $B_{n,x}$ component parallel to the external magnetic field should be considered (see Sec. III D 2). Similar to the previous sections, the nuclear spin fluctuation is considered to be frozen.

Magnetic field dependencies of the carrier spin polarization $-S_z^b$ and the signal phase are shown in Figs. 14(a) and 14(b) for different $\Delta\omega$ and $\tau_s/T_R = 300$. For a small frequency spread of $\Delta\omega = 0$ and $0.2\omega_R$, the polarization amplitude and phase are periodic functions of magnetic field, which is characteristic for the RSA regime [for comparison, see Figs. 5(b) and 5(d)]. An increase of $\Delta\omega$ to $0.5\omega_R$ drastically changes the character of these functions: both of them become independent of magnetic field. The spin polarization amplitude has a finite value (in this case it is equal 0.08), while $\phi = 0$. These are characteristics of the SML regime.

Details of separating the RSA from the SML regime with increasing frequency spread are presented in Fig. 14(c). The peak amplitudes of the spin polarization at the PSC frequencies are plotted for different pump pulse areas there. The amplitude initially decreases with an increasing spread and approaches a saturation level for larger spreads. Independence of the amplitude on the spread is characteristic for the SML regime, therefore, one can see from the Fig. 14(c) that the regimes cross over at $\Delta\omega \sim 0.5\omega_R$.

The spin polarization amplitude in the SML regime depends critically on the pump pulse area [see also Fig. 14(d)]. It is close to zero for $\Theta < 0.3\pi$, but strongly increases for Θ exceeding this value, approaching a maximum at $\Theta \to 2\pi$ for sufficiently large τ_s/T_R. The dependence of S_z^b for a large spread, which corresponds to a constant plateau level, can be written as

$$S_z^b = \frac{1-Q}{1+Q}\left[1 - \sqrt{\frac{M^2-1}{L^2-1}}\right], \tag{32}$$

where $M = Qe^{-T_R/\tau_s}$ and $L = e^{-T_R/\tau_s}(1+Q^2)/2$. The calculations in Fig. 14(d) show that with increasing electron spin relaxation time τ_s, the maximum signal amplitude shifts to a pulse area of 2π (unlike the dependence of spin polarization on pulse area for excitation by a single pulse, for which Rabi oscillations occur with maximum at $\Theta = \pi$).

The fact that the separation between RSA and SML is controlled by the ratio $\Delta\omega/\omega_R$ offers the instructive opportunity to realize a changeover between these two regimes by tuning the magnetic field. This would be possible for the case when the Larmor frequency spread is controlled by Δg (see Sec. III D 1) because in this case $\Delta\omega_g$ increases linearly with B. Results of corresponding calculations for $\Delta\omega_g = 0.1\omega_0$ are given in Fig. 15. In analogy with Figs. 14(a) and 14(b), one can identify the RSA regime in low magnetic fields ($|\omega_0/\omega_R| < 3$), where both the polarization amplitude and the phase change with B, and the SML regime in larger magnetic fields ($|\omega_0/\omega_R| > 5$), where these parameters do not vary anymore.

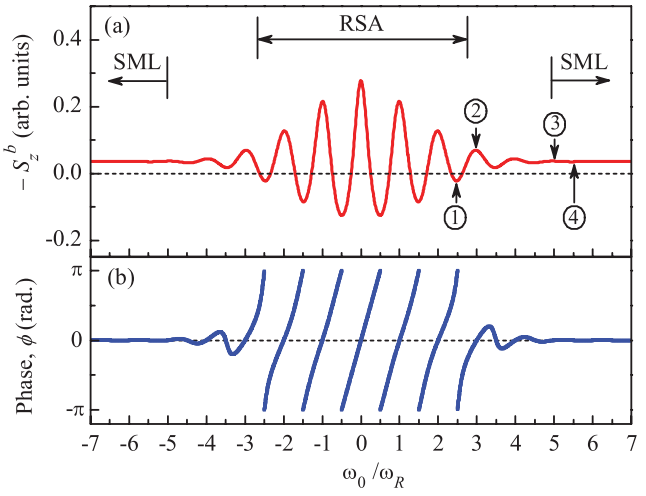

FIG. 15. (Color online) Magnetic field dependence of (a) carrier spin polarization $-S_z^b$ at zero pump-probe delay ($t \to 0^-$), and (b) spin precession phase of the signal calculated for the same parameters as in panel (a). The RSA and SML regimes are shown by arrows. The labels with numbers are in accordance with Fig. 16. $\tau_s/T_R = 3$, $\Theta = \pi$, $\Delta\omega_g = 0.1\omega_0$.

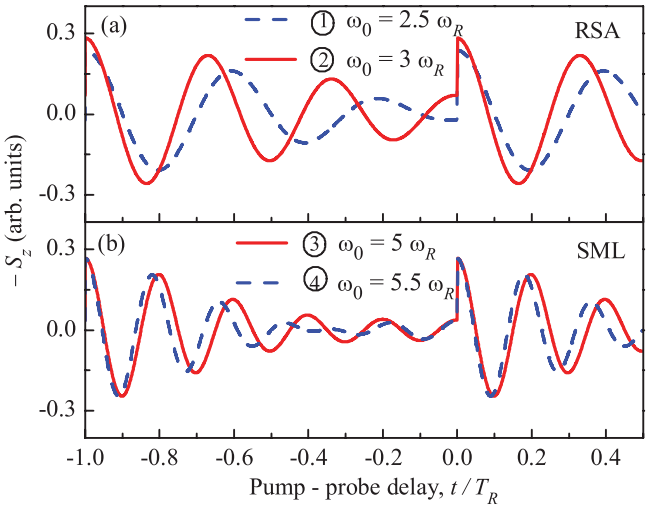

FIG. 16. (Color online) Carrier spin polarization as a function of pump-probe delay for different magnetic fields denoted in Fig. 15(a). Panel (a) corresponds to the RSA regime and panel (b) to the SML regime. $\tau_s/T_R = 3$, $\Theta = \pi$, $\Delta\omega_g = 0.1\omega_0$, $\tau_s^T \ll \tau_r$.

Figure 13(c) shows the range of parameters in which the different spin accumulation regimes can be obtained. The dashed curve corresponds to the condition $\Delta\omega = 0.5\omega_R$, which may serve as approximate boundary between the RSA and SML regimes. Indeed, if the g-factor spread is small, the spin-frequency distribution contains only one phase-synchronized mode in a broad range of magnetic fields, the latter are expressed via $\omega_0(B)/\omega_R$. It corresponds to the RSA regime for which the parameter space is placed below the dashed curve in Fig. 13(c). On the contrary, if the g-factor spread is large, several phase-synchronized modes become involved already at weak magnetic fields and, for relatively efficient optical pumping, SML occurs. It corresponds to the parameter space above the dashed curve in Fig. 13(c).

The time evolution of the spin polarization for the magnetic fields marked by numbers in Fig. 15(a) are given in Fig. 16. Figure 16(a) corresponds to the RSA regime (weak magnetic fields). One can see that the spin polarization phase and amplitude at small negative delays depend on the relation to the PSC. However, in the SML regime, shown in Fig. 16(b), both values are constant, irrespective of whether the PSC are fulfilled or not.

From the results of Secs. IV and V, one can conclude about the two main features of the SML regime. The first one is a fixed phase of the spin signal at very small negative delays, which is independent on the magnetic field. This reflects the primary amplification of spins with commensurable spin beat frequencies in a strongly inhomogeneous ensemble. The second one is a characteristic revival of the dephased signal before the next pump pulse arrival shown in Fig. 12.

It is also interesting that, in contrast with the RSA regime, in the SML regime the magnetic field dependence of the spin polarization at very small negative delay is smooth. The dependence is similar to that presented by the dashed line in Fig. 11(c). The width of this bell-like curve is determined by the nuclear field fluctuations and is approximately equal to $4\Delta_B$.

Let us summarize the conditions for the SML regime. Apart from the obvious condition $\tau_s \gg T_R$, it requires the following:

(1) A significant spread of carrier spin precession frequencies $\Delta\omega_g \gtrsim 0.5\omega_R$. The spread can be caused by the nuclear fluctuation fields or by the spread of g factors.

(2) The frequency spread $\Delta\omega \gtrsim 0.5\omega_R$ leads to a dephasing of the spin signal within the time $T_2^* \lesssim T_R/\pi$, i.e., faster than the time interval between subsequent pump pulses.

(3) One can see from Figs. 14(c) and 14(d) that the pump pulse area should be sufficiently large, $\Theta \gtrsim \pi/2$. Otherwise, the frequency spread $\Delta\omega \gtrsim 0.5\omega_R$ would cause only a decay of the spin polarization without its remarkable revival before the next pump pulse arrival.

VI. CONCLUSIONS

To conclude, we have performed a comprehensive theoretical study of carrier spin coherence in spin ensembles subject to periodic optical pumping. The effect of spin accumulation has been analyzed for singly charged quantum dots and quantum wells with a low density carrier gas. The accumulation results in two regimes of carrier spin coherence: resonance spin amplification and spin mode locking. These regimes, while being different in their phenomenological appearances and realization conditions, have the same origin and occur for spin ensembles for which the carrier spin coherence time exceeds by far the pump repetition period. The resonance spin amplification and spin mode locking are mutually exclusive regimes because of the requirement on excitation power and precession frequency spread.

For the RSA regime, sufficiently homogeneous spin ensembles and small excitation powers (small pump pulse areas) are required. These conditions are experimentally realized in QW structures with electron or hole resident carriers

of low density, i.e., for the regime, where negatively or positively charged trions play an important role. In this case, the spin dephasing times for resident carriers can be extracted with high accuracy, even when they exceed the pulse repetition period. The spreads of g factors and nuclear spin fluctuations are less important for the long-lived spin coherence compared to the case of strongly inhomogeneous QD ensembles.

In contrast to the RSA regime, the SML regime requires a strong inhomogeneity of the spin precession frequency in the spin ensemble and high excitation powers (pump areas close to π and more). By now, the SML regime has been observed experimentally and studied in great detail for ensembles of (In,Ga)As/GaAs QDs, each singly charged with a resident electron. In principle, it may be also observable for quantum dots singly charged with a resident hole, if the respective conditions are met.

ACKNOWLEDGMENTS

The authors thank A. Greilich, Al. L. Efros, I. V. Ignatiev, and E. L. Ivchenko for valuable discussions. This work was supported by the Deutsche Forschungsgemeinschaft, the Russian Foundation of Basic Research, and the EU Seventh Framework Programme (Grant No. 237252, Spin-optronics). I.A.Y. is a Fellow of the Alexander von Humboldt Foundation.

[1] *Semiconductor Spintronics and Quantum Computation*, edited by D. D. Awschalom, D. Loss, and N. Samarth (Springer, Berlin, 2002).

[2] *Optical Generation and Control of Quantum Coherence in Semiconductor Nanostructures*, Springer Series in NanoScience and Technology, edited by G. Slavcheva and Ph. Roussignol (Springer, Berlin, 2010).

[3] *Semiconductor Quantum Bits*, edited by F. Henneberger and O. Benson (Pan Stanford Publishing, Singapore, 2009).

[4] *Spin Physics in Semiconductors*, edited by M. Dyakonov (Springer, Berlin, 2008).

[5] J. M. Kikkawa and D. D. Awschalom, Phys. Rev. Lett. **80**, 4313 (1998).

[6] J. M. Kikkawa, I. P. Smorchkova, N. Samarth, and D. D. Awschalom, Science **277**, 1284 (1997).

[7] B. Beschoten, E. Johnston-Halperin, D. K. Young, M. Poggio, J. E. Grimaldi, S. Keller, S. P. DenBaars, U. K. Mishra, E. L. Hu, and D. D. Awschalom, Phys. Rev. B **63**, 121202 (2001).

[8] T. A. Kennedy, A. Shabaev, M. Scheibner, A. L. Efros, A. S. Bracker, and D. Gammon, Phys. Rev. B **73**, 045307 (2006).

[9] E. A. Zhukov, D. R. Yakovlev, M. Bayer, M. M. Glazov, E. L. Ivchenko, G. Karczewski, T. Wojtowicz, and J. Kossut, Phys. Rev. B **76**, 205310 (2007).

[10] W. J. H. Leyland, G. H. John, R. T. Harley, M. M. Glazov, E. L. Ivchenko, D. A. Ritchie, I. Farrer, A. J. Shields, and M. Henini, Phys. Rev. B **75**, 165309 (2007).

[11] J. A. Gupta, D. D. Awschalom, X. Peng, and A. P. Alivisatos, Phys. Rev. B **59**, R10421 (1999).

[12] J. A. Gupta, D. D. Awschalom, Al. L. Efros, and A. V. Rodina, Phys. Rev. B **66**, 125307 (2002).

[13] R. Epstein, D. T. Fuchs, W. V. Schoenfeld, P. M. Petroff, and D. D. Awschalom, Appl. Phys. Lett. **76**, 733 (2001).

[14] A. Greilich, D. R. Yakovlev, A. Shabaev, A. L. Efros, I. A. Yugova, R. Oulton, V. Stavarache, D. Reuter, A. Wieck, and M. Bayer, Science **313**, 341 (2006).

[15] A. Greilich, R. Oulton, E. A. Zhukov, I. A. Yugova, D. R. Yakovlev, M. Bayer, A. Shabaev, A. L. Efros, I. A. Merkulov, V. Stavarache, D. Reuter, and A. Wieck, Phys. Rev. Lett. **96**, 227401 (2006).

[16] A. Greilich, M. Wiemann, F. G. G. Hernandez, D. R. Yakovlev, I. A. Yugova, M. Bayer, A. Shabaev, Al. L. Efros, D. Reuter, and A. D. Wieck, Phys. Rev. B **75**, 233301 (2007).

[17] *Optical Orientation*, edited by F. Meier and B. P. Zakharchenya (North-Holland, Amsterdam, 1984).

[18] J. Berezovsky, M. H. Mikkelsen, N. G. Stoltz, L. A. Coldren, and D. D. Awschalom, Science **320**, 349 (2008).

[19] M. Atature, J. Dreiser, A. Badolato, and A. Imamoglu, Nat. Phys. **3**, 101 (2007).

[20] A. Greilich, D. R. Yakovlev, and M. Bayer, in *Optical Generation and Control of Quantum Coherence in Semiconductor Nanostructures*, edited by G. Slavcheva and Ph. Roussignol (Springer, Berlin, 2010), Chap. 6, pp. 85–127.

[21] D. R. Yakovlev and M. Bayer, in *Spin Physics in Semiconductors*, edited by M. I. Dyakonov (Springer, Berlin, 2008), Chap. 6, pp. 135–177.

[22] L. V. Fokina, I. A. Yugova, D. R. Yakovlev, M. M. Glazov, I. A. Akimov, A. Greilich, D. Reuter, A. D. Wieck, and M. Bayer, Phys. Rev. B **81**, 195304 (2010).

[23] I. A. Yugova, M. M. Glazov, E. L. Ivchenko, and A. L. Efros, Phys. Rev. B **80**, 104436 (2009).

[24] S. Spatzek, S. Varwig, M. M. Glazov, I. A. Yugova, A. Schwan, D. R. Yakovlev, D. Reuter, A. D. Wieck, and M. Bayer, Phys. Rev. B **84**, 115309 (2011).

[25] M. M. Glazov, Fiz. Tverd. Tela **54**, 3 (2012) [Phys. Solid State **54**, 1 (2012)].

[26] A. Shabaev, A. L. Efros, D. Gammon, and I. A. Merkulov, Phys. Rev. B **68**, 201305 (2003).

[27] N. H. Bonadeo, J. Erland, D. Gammon, D. Park, D. S. Katzer, and D. G. Steel, Science **282**, 1473 (1998).

[28] E. A. Zhukov, D. R. Yakovlev, M. M. Glazov, L. Fokina, G. Karczewski, T. Wojtowicz, J. Kossut, and M. Bayer, Phys. Rev. B **81**, 235320 (2010).

[29] An ensemble of electron spins in magnetic field can be characterized by three relaxation times [see A. Abragam, *The Principles of Nuclear Magnetism* (Oxford University Press, Oxford, 1961), p. 44.]: the longitudinal spin relaxation time T_1, which is related to the relaxation of the spin component parallel to the field (S_x in our case), and the transverse spin relaxation times T_2 and T_2^*. The T_2 time describes spin decoherence (i.e., relaxation of the spin components transverse to the field: S_y and S_z in our notation) of a single carrier, while the T_2^* time describes the dephasing of the spin ensemble (e.g., due to the inhomogeneous broadening of the carrier g factor). Due to the anisotropy of spin relaxation in QWs (Refs. 45–48), the spin relaxation times T_y and T_z differ from each

other. In Eqs. (5), we assume for simplicity an isotropic relaxation time: $\tau_s = T_x = T_y = T_z$. The effect of spin dephasing anisotropy is considered in Sec. III C.

[30] I. Y. Gerlovin, Y. P. Efimov, Y. K. Dolgikh, S. A. Eliseev, V. V. Ovsyankin, V. V. Petrov, R. V. Cherbunin, I. V. Ignatiev, I. A. Yugova, L. V. Fokina, A. Greilich, D. R. Yakovlev, and M. Bayer, Phys. Rev. B **75**, 115330 (2007).

[31] The situation is typical for n-type structures with resident electrons, where the T^- trion spin dynamics is controlled by the hole spin. This is related to the fact that in QWs and epitaxially grown QDs, the in-plane g factor of the heavy hole is close to zero and, therefore, one can neglect the hole Larmor precession, i.e., $\Omega = 0$, to a good approximation.

[32] X. Marie, T. Amand, P. Le Jeune, M. Paillard, P. Renucci, L. E. Golub, V. D. Dymnikov, and E. L. Ivchenko, Phys. Rev. **60**, 5811 (1999).

[33] I. A. Yugova, I. Ya. Gerlovin, V. G. Davydov, I. V. Ignatiev, I. E. Kozin, H.-W. Ren, M. Sugisaki, S. Sugou, and Y. Masumoto, Phys. Rev. B **66**, 235312 (2002).

[34] R. M. Stevenson, R. J. Young, P. See, D. G. Gevaux, K. Cooper, P. Atkinson, I. Farrer, D. A. Ritchie, and A. J. Shields, Phys. Rev. B **73**, 033306 (2006).

[35] P. Machnikowski and T. Kuhn, Phys. Rev. B **81**, 115306 (2010).

[36] T. Korn, M. Kugler, M. Griesbeck, R. Schulz, A. Wagner, M. Hirmer, C. Gerl, D. Schuh, W. Wegscheider, and C. Schüller, New J. Phys. **12**, 043003 (2010).

[37] B. Beschoten, Spin Coherence in Semiconductors in Magnetism goes Nano, 36th Spring School 2005, Schriften des Forschungzentrums Jülich, Matter and Materials (unpublished).

[38] M. M. Glazov and E. L. Ivchenko, Sov. Phys. Semicond. **42**, 951 (2008) [Fiz. Techn. Polupr. **42**, 966 (2008)].

[39] Strictly speaking, the dephasing time of a spin ensemble T_2^* is magnetic field dependent due to the spread of carrier g factors (see Sec. III D). The effect of the peak broadening for an increasing magnetic field (that is with an increase of the peak number N) is analyzed in Sec. III D.

[40] G. V. Astakhov, M. M. Glazov, D. R. Yakovlev, E. A. Zhukov, W. Ossau, L. W. Molenkamp, and M. Bayer, Semicond. Sci. Technol. **23**, 114001 (2008).

[41] E. A. Zhukov, D. R. Yakovlev, M. Bayer, G. Karczewski, T. Wojtowicz, and J. Kossut, Phys. Status Solidi B **243**, 878 (2006).

[42] I. A. Yugova, A. A. Sokolova, D. R. Yakovlev, A. Greilich, D. Reuter, A. D. Wieck, and M. Bayer, Phys. Rev. Lett. **102**, 167402 (2009).

[43] A. Greilich, S. Spatzek, I. A. Yugova, I. A. Akimov, D. R. Yakovlev, A. L. Efros, D. Reuter, A. D. Wieck, and M. Bayer, Phys. Rev. B **79**, 201305(R) (2009).

[44] M. Kugler, K. Korzekwa, P. Machnikowski, C. Gradl, S. Furthmeier, M. Griesbeck, M. Hirmer, D. Schuh, W. Wegscheider, T. Kuhn, C. Schüller, and T. Korn, Phys. Rev. B **84**, 085327 (2011).

[45] M. I. Dyakonov and V. Yu. Kachorovskii, Sov. Phys. Semicond. **20**, 110 (1986) [Fiz. Techn. Polupr. **20**, 178 (1986)].

[46] N. S. Averkiev and L. E. Golub, Phys. Rev. B **60**, 15582 (1999).

[47] N. S. Averkiev, L. E. Golub, A. S. Gurevich, V. P. Evtikhiev, V. P. Kochereshko, A. V. Platonov, A. S. Shkolnik, and Y. P. Efimov, Phys. Rev. B **74**, 033305 (2006).

[48] A. V. Larionov and L. E. Golub, Phys. Rev. B **78**, 033302 (2008).

[49] N. S. Averkiev, L. E. Golub, and M. Willander, J. Phys.: Condens. Matter **14**, R271 (2002).

[50] M. Griesbeck, M. M. Glazov, E. Ya. Sherman, D. Schuh, W. Wegscheider, C. Schüller, and T. Korn, Phys. Rev. B **85**, 085313 (2012).

[51] M. Ikezawa, B. Pal, Y. Masumoto, I. V. Ignatiev, S. Y. Verbin, and I. Y. Gerlovin, Phys. Rev. B **72**, 153302 (2005).

[52] A. V. Khaetskii and Y. V. Nazarov, Phys. Rev. B **64**, 125316 (2001).

[53] L. M. Woods, T. L. Reinecke, and Y. Lyanda-Geller, Phys. Rev. B **66**, 161318 (2002).

[54] S. G. Carter, A. Shabaev, S. E. Economou, T. A. Kennedy, A. S. Bracker, and T. L. Reinecke, Phys. Rev. Lett. **102**, 167403 (2009).

[55] E. L. Ivchenko, *Optical Spectroscopy of Semiconductor Nanostructures* (Alpha Science, Harrow, UK, 2005).

[56] I. A. Yugova, A. Greilich, D. R. Yakovlev, A. A. Kiselev, M. Bayer, V. V. Petrov, Y. K. Dolgikh, D. Reuter, and A. D. Wieck, Phys. Rev. B **75**, 245302 (2007).

[57] R. Kotlyar, T. L. Reinecke, M. Bayer, and A. Forchel, Phys. Rev. B **63**, 085310 (2001).

[58] I. A. Merkulov, A. L. Efros, and M. Rosen, Phys. Rev. B **65**, 205309 (2002).

[59] M. Syperek, D. R. Yakovlev, I. A. Yugova, J. Misiewicz, I. V. Sedova, S. V. Sorokin, A. A. Toropov, S. V. Ivanov, and M. Bayer, Phys. Rev. B **84**, 085304 (2011); **84**, 159903(E) (2011).

[60] If the spreads of g factors and nuclear spin fluctuation fields are described by normal distributions (Gaussians), then the dispersion of electron spin precession frequencies in the QD ensemble is (Ref. 43) $\Delta\omega = \sqrt{(\Delta g \mu_B B/\hbar)^2 + \omega_n^2}$. This leads to a Gaussian dephasing with a characteristic time $T_2^* = 1/\Delta\omega$.

[61] M. Yu. Petrov, I. V. Ignatiev, S. V. Poltavtsev, A. Greilich, A. Bauschulte, D. R. Yakovlev, and M. Bayer, Phys. Rev. B **78**, 045315 (2008).

[62] The zeroth RSA peak [Eq. (19)] has the same form as the standard expression for the Hanle effect (Ref. 17): the electron spin depolarization in a transversal magnetic field under continuous-wave pumping. The influence of the inhomogeneous distribution of g factors on the Hanle effect is typically quite weak and, as a rule (Refs. 40 and 63), the extracted spin dephasing time is controlled by the nuclear spin fluctuations, i.e., by T_2^*. As compared with the Hanle effect, the studies of the resonant spin amplification allow one to directly extract the magnetic field dependence of the spin dephasing time and, consequently, evaluate the spread of g factors Δg.

[63] S. V. Andreev, B. R. Namozov, A. V. Koudinov, Yu. G. Kusrayev, and J. K. Furdyna, Phys. Rev. B **80**, 113301 (2009).